CANADIAN THESES ON MICROFICHE

THÈSES CANADIENNES SUR MICROFICHE

National Library of Canada
Collections Development Branch

Canadian Theses on
Microfiche Service

Ottawa, Canada
K1A 0N4

Bibliothèque nationale du Canada
Direction du développement des collections

Service des thèses canadiennes
sur microfiche

NOTICE

The quality of this microfiche is heavily dependent upon the quality of the original thesis submitted for microfilming. Every effort has been made to ensure the highest quality of reproduction possible.

If pages are missing, contact the university which granted the degree.

Some pages may have indistinct print especially if the original pages were typed with a poor typewriter ribbon or if the university sent us an inferior photocopy.

Previously copyrighted materials (journal articles, published tests, etc.) are not filmed.

Reproduction in full or in part of this film is governed by the Canadian Copyright Act, R.S.C. 1970, c. C-30. Please read the authorization forms which accompany this thesis.

AVIS

La qualité de cette microfiche dépend grandement de la qualité de la thèse soumise au microfilmage. Nous avons tout fait pour assurer une qualité supérieure de reproduction.

S'il manque des pages, veuillez communiquer avec l'université qui a conféré le grade.

La qualité d'impression de certaines pages peut laisser à désirer, surtout si les pages originales ont été dactylographiées à l'aide d'un ruban usé ou si l'université nous a fait parvenir une photocopie de qualité inférieure.

Les documents qui font déjà l'objet d'un droit d'auteur (articles de revue, examens publiés, etc.) ne sont pas microfilmés.

La reproduction, même partielle, de ce microfilm est soumise à la Loi canadienne sur le droit d'auteur, SRC 1970, c. C-30. Veuillez prendre connaissance des formules d'autorisation qui accompagnent cette thèse.

THIS DISSERTATION
HAS BEEN MICROFILMED
EXACTLY AS RECEIVED

LA THÈSE A ÉTÉ
MICROFILMÉE TELLE QUE
NOUS L'AVONS REÇUE

Canada

NL 339 (r. 86/09)

THE IMPATT AMPLIFIER IN FIN LINE

MILES BURTON

A thesis submitted in partial fulfillment
of the requirements for the degree
Master of Applied Science

Department of Electrical Engineering
University of Ottawa
June, 1985

ABSTRACT

This thesis deals with the theoretical and practical aspects of negative-resistance amplifier design in high-impedance environments such as fin line. To support the analysis, an IMPATT amplifier in single-ridge fin line is designed, and the amplifier's performance is measured. Both analysis and experiment show that the behavior of negative-resistance amplifiers in high-impedance environments is very sensitive to changes in circuit parameters. Also, the design of such amplifiers is shown to require excessive accuracy in the characterization of the diode as the diode reflection-coefficient approaches the unit circle, and as the required gain increases.

The equalizer design for the fin-line amplifier was based on an improved characterization of series stubs in fin line. This characterization is presented in the form of empirical closed-form expressions for the scattering parameters of series stubs in single-ridge unilateral fin line with narrow gap width. These expressions show the effect of fin-line gap-width, stub length and frequency, and are suitable for computer-aided design.

ACKNOWLEDGEMENT

The author gratefully acknowledges the advice and guidance received from Dr. W.J.R. Hoefer during this study.

TABLE OF CONTENTS

TABLE OF CONTENTS (CONTINUED)

1-1 INTRODUCTION

Activity in the millimeter-wave spectrum continues to increase to meet civilian, scientific, and military needs in such diverse fields as satellite communications, remote sensing and terminal seekers for missiles. The mm-wave circuit designer must draw from a wide range of technologies to meet specifications that are unique to each application. For applications requiring moderate power amplifiers in moderate production quantities, the IMPATT amplifier in fin line technique promises to be a light weight, low cost realization.

At mm-wave frequencies the IMPATT diode is the most powerful and most efficient solid state device. Where the benefits of solid state (low cost, light weight, and low-voltage power supply) are essential, the IMPATT amplifier is preferred if its limitations (limited bandwidth, poor linearity, high noise, inadequate efficiency, and poor temperature stability) can be tolerated.

The small dimensions and associated tight tolerances of mm-wave circuits are much costlier to realize with conventional waveguide structures than with the printed-circuit structures of fin line or microstrip. At mm-wave frequencies, fin line is often preferred over microstrip because it has less severe tolerances, it has lower losses, it is naturally shielded, and it allows straightforward transitions to waveguide.

Thus, the special features of both the IMPATT diode and the fin line should combine to make a light weight and inexpensive moderate power amplifier.

This thesis records an attempt to demonstrate the viability of IMPATT amplifiers in a fin-line environment. It describes both the theory and the experimental procedures that were used to construct an amplifier operating at 11 GHz. This low frequency allows the convenience of larger dimensions and more precise

network analyser measurements; yet it does not prevent the techniques used and the lessons learned from being applied to higher frequencies.

2-1 AN OVERVIEW OF NEGATIVE-RESISTANCE AMPLIFIERS

The negative-resistance (or regenerative) amplifier is commonly used at frequencies where transistors with the required output power are nonexistent. The inherent isolation, high gain, simplicity and wide bandwidth of the transistor amplifier are sacrificed for the higher power of the negative-resistance amplifier circuit.

The negative-resistance device is usually a packaged semiconductor diode (IMPATT, Gunn, etc.) that behaves like a lumped immittance with a negative real part. For example, a typical silicon IMPATT diode operating at 11 Ghz would present about -2 -j12 ohms at the package terminals when biased with a direct current of 200 mA. A good general description of negative-resistance devices as well as a comprehensive list of references is given in [1].

Fig. 2-1 shows functional diagrams for the two basic types of negative-resistance amplifiers : reflection amplifiers and transmission amplifiers. In the reflection amplifier (Fig. 2-1a), the output power is the power reflected from the equalizer and the gain is $|\Gamma_{in}|^2$, the squared magnitude of the reflection coefficient at the equalizer input. In the transmission amplifier (Fig. 2-1b), the output power is the transmitted power and the gain is the squared magnitude of the overall transmission coefficient.

The equalizers in both types are lossless, partially reflective circuits that are designed to increase the magnitude of the appropriate diode S-parameter (reflection coefficient or transmission coefficient) to that required for the complete amplifier. This increase is obtained at the expense of reduced useable bandwidth.

Single-diode reflection amplifiers are nonreciprocal because

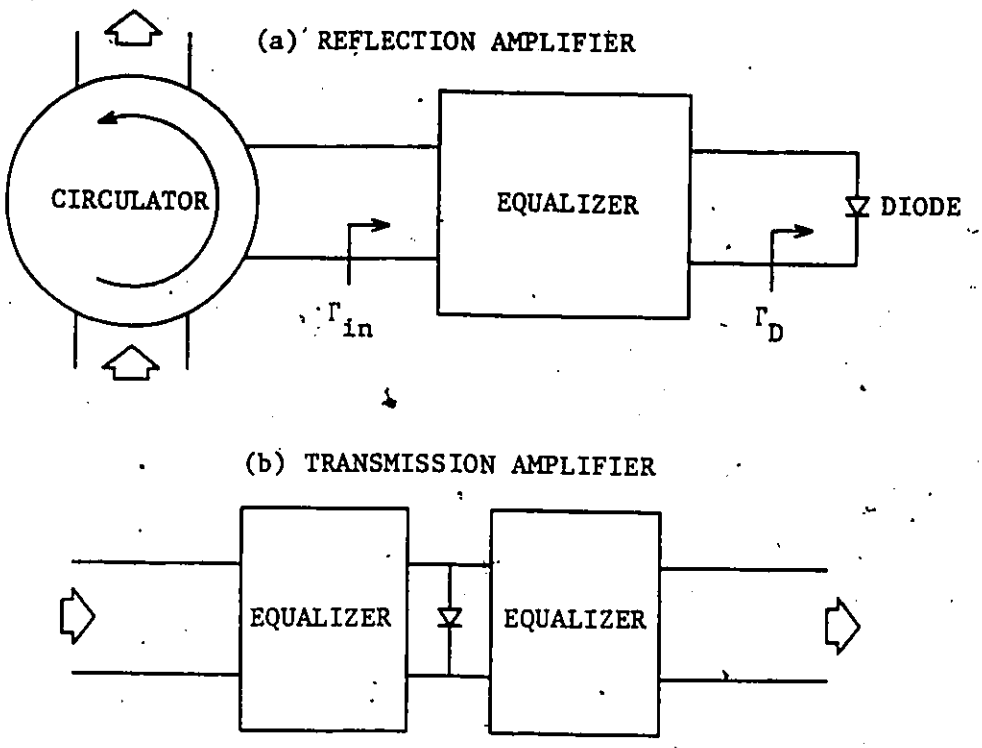

Fig. 2-1 The two basic types of reflection amplifier.

they use a circulator to separate the input and output signals. The bandwidth is usually that of the circulator, which is typically less than 5 percent for low insertion loss (less than 0.5 dB) types for mm-wave frequencies [2]. The circulator can be eliminated if two reflection amplifiers are coupled through a 90^{o} hybrid circuit as shown in Fig. 2-2. The gain is the same as for either amplifier but the output power is doubled. The hybrid-coupled amplifier is reciprocal and its bandwidth is that of either individual amplifier. However, if the load and generator must be isolated, the bandwidth is reduced to that of the necessary isolator(s), which is typically the same as for the circulators mentioned above. Reference [3] contains a 1979 survey of millimeter-wave solid-state reflection amplifiers as well as a large list of references.

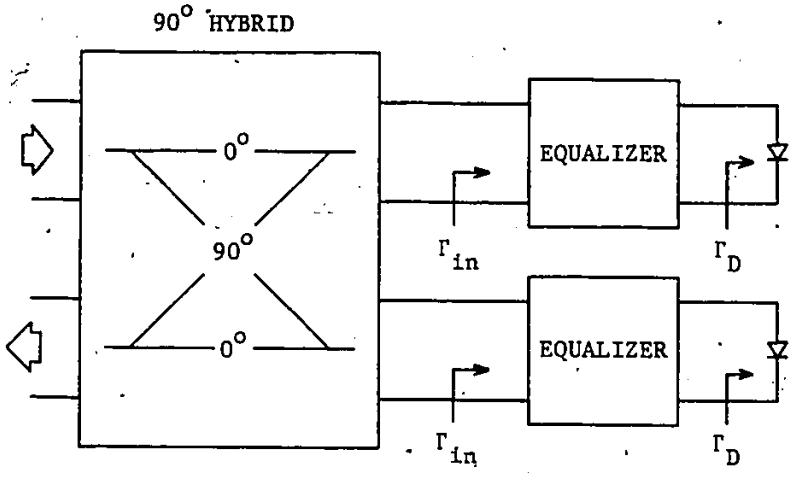

Fig. 2-2 The hybrid coupled reflection amplifier is reciprocal.

The transmission amplifier has no inherent need for a circulator. Therefore it has a greater potential bandwidth than the reflection amplifier. However, like the hybrid-coupled amplifier, the transmission amplifier is reciprocal, and the bandwidth suffers when isolators are added. Also, this amplifier type tends to exhibit reflection gain which can rise to levels significantly higher than unity at the passband edges. Three-stage transmission amplifiers without interstage isolators have been demonstrated [4].

The negative resistance of diodes decreases quickly (towards zero) as the incident power increases. In an IMPATT amplifier designed for maximum output power, the diode's negative resistance is about one-third of its small signal value. This nonlinear characteristic can cause the amplifier to oscillate when the input signal is removed. Such an amplifier is called an injection-locked oscillator because it can be considered as an oscillator whose frequency will lock to that of the "injected" input signal (when that signal is sufficiently large).

Amplifiers that don't oscillate when the input signal is removed are said to be stable. A more detailed description of the injection locked oscillator type of amplifier is given in Sec. 5-2.

IMPATT diodes are the most powerful source of solid state power but they also have the largest noise figures. Consequently, this type of diode is most often used in the final stage of a cascade of amplifiers where the additional noise is least detrimental. IMPATT amplifiers for this application are usually injection locked. See reference [5] for an example.

The fin-line amplifier that was designed for this thesis was a stable reflection-type IMPATT amplifier since it was not possible to obtain in the lab the necessary large input signal levels for injection locking. The diode was characterized and the amplifier was tested with network analyser signals of much less power (~5 μW) than the maximum power available from the diode (~3 W).

2-2 REFERENCES

[1] L.O.Chua et al, "Bipolar-JFET-MOSFET negative resistance devices," IEEE Trans. Circuits Syst., vol. CAS-32, pp. 46-61, Jan. 1985.

[2] Hughes Aircraft Co.: 1983 Catalog, Solid State Millimeter-wave Products, pp. 61-63.

[3] B.A.Kotserzhinskii et al, "Millimetre band solid-state reflection amplifiers," Izvestiya VUZ. Radioelektronika, vol. 22, No. 10, pp. 30-43, 1979. Available in english from CISTI as an Allerton Press, Inc. reproduction,

[4] H.C.Bowers et al, "IMPATT-diode multistage transmission amplifiers," IEEE Trans. Microwave Theory Tech., vol. MTT-18, pp. 943-951, Nov. 1970.

[5] V.Sokolov et al, "A 4-W 56-dB gain microstrip amplifier at 15 GHz utilizing GaAs FET's and IMPATT diodes," IEEE Trans. Microwave Theory Tech., vol MTT-27, pp. 1058-1065, Dec. 1979.

3-1 SOME REFLECTION AMPLIFIER THEORY

The basic reflection amplifier is a cascade connection of two circuits: the equalizer, and the negative-resistance device. The interplay of signals in such a circuit can be easily determined with the aid of a signal flow graph like the one in Fig. 3-1.

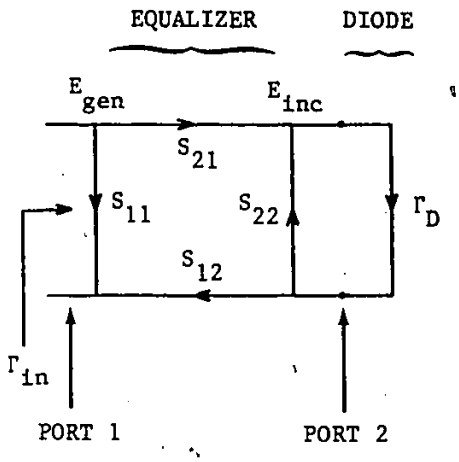

Fig. 3-1 The signal flow graph for the basic reflection amplifier.

Each of the symbols E_{gen} and E_{inc} in the figure represents the complex amplitude of the total signal at the node which is adjacent to the symbol. The magnitude is equal to the square root of the signal power. The phase is equal to the phase of the signal.

Whenever two circuits are connected in cascade, the loop equation for the signals at the interface must be satisfied. From Fig. 3-1 the loop equation for the reflection amplifier is

$$E_2 + E_{inc}\Gamma_D S_{22} = E_{inc} \qquad (3\text{-}1a)$$

where $E_2 = E_{gen}S_{21}$ (3-1b)

Suppose the input signal is removed so that $E_{gen} = 0$. If E_{inc} is subsequently discovered to be nonzero, then the circuit is an oscillator by definition and eq. (3-1a) simplifies to

$$\Gamma_D S_{22} = 1 \tag{3-2}$$

(3-2) is notationally very simple but not as informative as the equivalent eq. (3-3).

$$\arg[S_{22}] = -\arg[\Gamma_D] \tag{3-3a}$$

$$|S_{22}| = 1/|\Gamma_D| \tag{3-3b}$$

These equations give the phase and magnitude relationships that prevail when the circuit is oscillating.

When E_{gen} is nonzero, the circuit is a reflection amplifier and (3-3b) is no longer correct. However, (3-3a) remains at least approximately correct throughout the amplifier passband. This will now be demonstrated by showing that $|E_2|$ is much less than $|E_{inc}|$ in a typical amplifier:

Since the equalizer in Fig. 3-1 is nearly lossless, the power added by the diode can be measured at either equalizer port as the difference between the power flowing left and the power flowing right. At port 2, the power added is

$$P_{add} = P_{inc}|\Gamma_D|^2 - P_{inc} = P_{inc}(|\Gamma_D|^2 - 1) \tag{3-4}$$

where P_{inc} is the power incident on the diode.

At port 1, the power added is

$$P_{add} = P_{gen}G - P_{gen} = P_{gen}(G - 1) \tag{3-5}$$

where G is the amplifier gain, and P_{gen} is the power incident on port 1 of the equalizer.

(3-4) and (3-5) can be combined to eliminate P_{add} and obtain a relationship between the power incident on the diode, P_{inc}, and the power incident on the amplifier, P_{gen}. The result is

$$P_{inc} = \frac{(G - 1)P_{gen}}{|\Gamma_D|^2 - 1} \qquad (3\text{-}6)$$

Since the equalizer is lossless, its S-parameters obey the relationships (3-7) [1].

$$|S_{11}| = |S_{22}| \qquad (3\text{-}7a)$$

$$|S_{21}| = |S_{12}| \qquad (3\text{-}7b)$$

$$S_{21}S_{12} = -[1 - |S_{11}|^2] \exp(j\{\arg[S_{11}] + \arg[S_{22}]\}) \qquad (3\text{-}7c)$$

(Note that in [1] the authors define the ingoing and outgoing travelling waves as voltage waves with complex amplitudes of $a = V_{in}$ and $b = V_{out}$, resp. If the more popular definitions of $a = V_{in}/\sqrt{Z_o}$ and $b = V_{out}/\sqrt{Z_o}$ are used, then the relations given in [1] reduce to eqs. (3-7), which are independent of the characteristic impedance at either port.)

By applying eqs. (3-7) to (3-1b), the power leaving port 2 when the equalizer is perfectly matched can be computed as

$$\begin{aligned} P_2 &= P_{gen}|S_{21}|^2 \\ &= P_{gen}|S_{21}S_{12}| \\ &= P_{gen}(1 - |S_{11}|^2) \\ &= P_{gen}(1 - |S_{22}|^2) \end{aligned} \qquad (3\text{-}8)$$

To relate the power incident on the diode to the power that would be incident on a matched load, (3-6) and (3-8) can be combined to obtain

$$\frac{P_{inc}}{P_2} = \frac{(G - 1)}{(|\Gamma_D|^2 - 1)(1 - |S_{22}|^2)} \qquad (3\text{-}9)$$

An alternative and independent solution for P_{inc}/P_2 can be obtained by rearranging (3-1a) to give

$$\frac{E_{inc}}{E_2} = \frac{1}{1 - \Gamma_D S_{22}} \qquad (3\text{-}10)$$

The corresponding ratio of the powers is just

$$\frac{P_{inc}}{P_2} = \frac{1}{|1 - \Gamma_D S_{22}|^2} \qquad (3\text{-}11)$$

This equation and (3-9) can be combined to give

$$|1 - \Gamma_D S_{22}|^2 = K(1 - |S_{22}|^2) \qquad (3\text{-}12)$$

where $K = \dfrac{|\Gamma_D|^2 - 1}{G - 1}$

Although (3-12) does not uniquely determine S_{22}, it does establish upper and lower limits for $|S_{22}|$. (See Appendix 5.) These limits are

$$|S_{22}| = \frac{|\Gamma_D| \pm (K^2 + |\Gamma_D|^2 K - K)^{1/2}}{|\Gamma_D|^2 + K} \qquad (3\text{-}13)$$

In the passband of a reflection amplifier, typical values for G, and $|\Gamma_D|$ are:

$$G = 4 \qquad (3\text{-}14a)$$

$$|\Gamma_D| = 1.1 \qquad (3\text{-}14b)$$

For these values, $|S_{22}|$ must be in the range

$$0.75 \leq |S_{22}| \leq 0.96875 \qquad (3\text{-}14c)$$

In (3-9) the ratio P_{inc}/P_2 can be no smaller than the value set by the smallest value of $|S_{22}|$. Substituting $|S_{22}| = 0.75$ and eqs. (3-14a,b) into (3-9) gives

$$P_{inc} \geq 33\ P_2 \qquad (3\text{-}15)$$

or, equivalently,

$$|E_2| \leq 33^{1/2}\ |E_{inc}| \qquad (3\text{-}16)$$

Since $|E_2|$ is much smaller than $|E_{inc}|$ in the passband of a reflection amplifier, one can say that

$$\arg[\Gamma_D S_{22}] \simeq 0 \qquad (3\text{-}17)$$

Generally the phases of both Γ_D and S_{22} decrease monotonically with frequency so that, at some frequency f_c near the center of the passband, $\arg[\Gamma_D S_{22}]$ is exactly zero and (3-17) is replaced by (3-3a).

Eq. (3-17) establishes $\arg[S_{22}]$ in the passband. A formula for $|S_{22}|$ in the passband will now be derived:

Mason's loop rule [2] can be applied to the signal flow graph in Fig. 3-1 to get the familiar relation

$$\Gamma_{in} = S_{11} + \frac{S_{21}S_{12}\Gamma_D}{1 - S_{22}\Gamma_D} \tag{3-18}$$

Since the equalizer is lossless, eqs. (3-7) can be applied to (3-18) to obtain

$$\Gamma_{in} = \frac{|S_{22}| - \Gamma_D \exp(j\arg[S_{22}])}{1 - S_{22}\Gamma_D} \exp(j\arg[S_{11}]) \tag{3-19}$$

This can be simplified with the aid of (3-17) to obtain

$$\Gamma_{in} \simeq \frac{|S_{22}| - |\Gamma_D|}{1 - |S_{22}||\Gamma_D|} \exp(j\arg[S_{11}]) \tag{3-20}$$

which is exact when the frequency is f_c. Taking the magnitude of both sides of (3-20) and solving for $|S_{22}|$ gives

$$|S_{22}| \simeq \frac{|\Gamma_D| - |\Gamma_{in}|}{1 - |\Gamma_D||\Gamma_{in}|} \tag{3-21}$$

Since the gain of the amplifier is $G=|\Gamma_{in}|^2$, one can replace $|\Gamma_{in}|$ in eq. (3-21) with $G^{1/2}$ to give

$$|S_{22}| \simeq \frac{|\Gamma_D| - G^{1/2}}{1 - |\Gamma_D|G^{1/2}} \tag{3-22}$$

which is exact at f_c. This equation is useful in equalizer

design and in the sensitivity analysis that follows next.

3-2 SENSITIVITY ANALYSIS

The characteristics of the components of a reflection amplifier can vary from their assumed values because of ageing, environmental changes, experimental error, etc. These variations can cause the amplifier to depart significantly from its desired behavior. Thus, it is important to know in advance the sensitivity of Γ_{in} to changes in Γ_D. This section will show that the sensitivity of Γ_{in} to Γ_D is strongly dependent on the characteristic impedance of the transmission line in which the diode is mounted.

The sensitivity of Γ_{in} to Γ_D is defined as

$$S = \frac{\Gamma_D}{\Gamma_{in}} \frac{d\Gamma_{in}}{d\Gamma_D} \tag{3-23}$$

This can be evaluated by the direct substitution of (3-19), but the process is somewhat simplified by writing (3-19) as

$$\Gamma_{in} = \Gamma \exp(j\arg[S_{11}]) \tag{3-24a}$$

$$\text{where } \Gamma = \frac{|S_{22}| - \Gamma_D \exp(j\arg[S_{22}])}{1 - S_{22}\Gamma_D} \tag{3-24b}$$

Because Γ and Γ_{in} are related by a constant factor that is independent of Γ_D, the sensitivities of both Γ_{in} and Γ to Γ_D are identical. Thus S can be computed simply as

$$S = \frac{\Gamma_D}{\Gamma}\,\frac{d\Gamma}{d\Gamma_D} \tag{3-25}$$

Since Γ is an analytic function of Γ_D, obtaining its complex derivative is straightforward. It is

$$d\Gamma/d\Gamma_D = \frac{(|S_{22}|^2 - 1)\exp(j\arg[S_{22}])}{(1 - S_{22}\Gamma_D)^2} \tag{3-26}$$

Substituting (3-26) and (3-24b) into (3-25) gives

$$S = \frac{(|S_{22}|^2 - 1)\exp(j\arg[S_{22}])}{1 - S_{22}\Gamma_D}\,\frac{\Gamma_D}{|S_{22}| - \Gamma_D\exp(j\arg[S_{22}])} \tag{3-27}$$

This is exact for all frequencies. In the passband, (3-17) is true and S can be approximated by

$$S \simeq \frac{|S_{22}|^2 - 1}{1 - |S_{22}||\Gamma_D|}\,\frac{|\Gamma_D|}{|S_{22}| - |\Gamma_D|} \tag{3-28}$$

which is exact at the frequency f_c. Thus S is real at f_c and can be expected to be nearly real elsewhere in the passband. Also, (3-22) is exact at f_c. Thus S depends only on $|\Gamma_D|$ and G at f_c and can be expected to be relatively insensitive to $\arg[\Gamma_D]$ and S_{22} in the rest of the passband.

The behavior of (3-28) at f_c is shown in Fig. 3-2 where S is plotted as a function of $|\Gamma_D|$ for various passband gains. The figure shows that the sensitivity will increase as the gain increases and as $|\Gamma_D|$ decreases. In fact, as $|\Gamma_D|$ approaches unity, the sensitivity becomes infinite. In other words, as $|\Gamma_D|$ approaches unity, even a very small

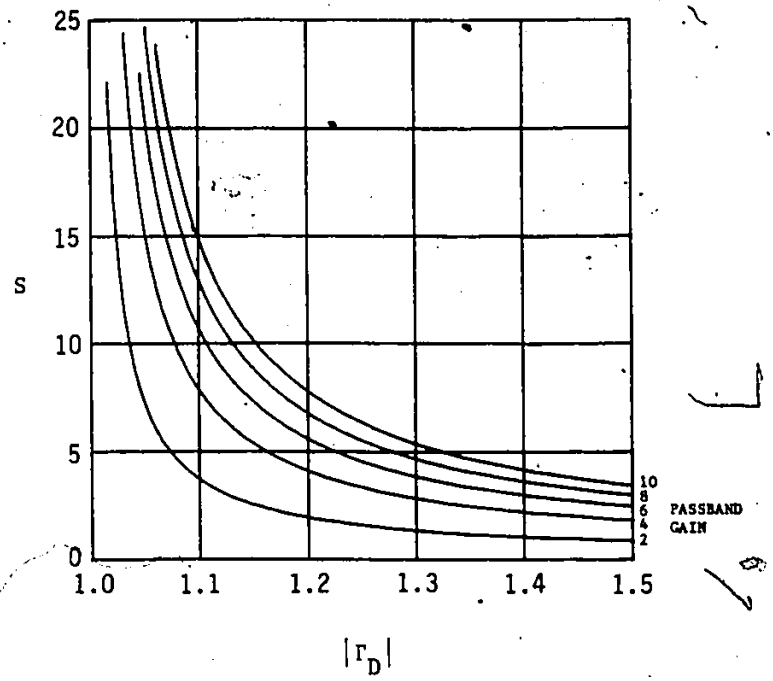

Fig. 3-2 The sensitivity S of Γ_{in} to Γ_D as a function of $|\Gamma_D|$ for various passband gains.

uncertainty in Γ_D will make the design totally unpredictable.

Another way to illustrate the uncertainty in Γ_{in} due to a given uncertainty in Γ_D is based on the bilinear nature of (3-19). This equation has the property of mapping circles in the Γ_D plane into circles in the Γ_{in} plane. In particular it will map an error circle for Γ_D into the corresponding error circle for Γ_{in}.

Suppose that at the frequency f_c, an amplifier has an assumed value of $\Gamma_D = -1.06 - j0.28$, and that the anticipated gain is G = 4. Suppose also that the actual value of Γ_D lies on the circumference of a circle of radius 0.03 centered on the assumed value for Γ_D. The size and location of the

corresponding error circle for Γ_{in} can be obtained from the formulas in Appendix 2, which relate the centers and radiuses of bilinearly transformed circles. One need only use (3-17) and (3-22) to obtain a value for S_{22} in the bilinear transformation (3-19). The two circles are plotted in Fig. 3-3.

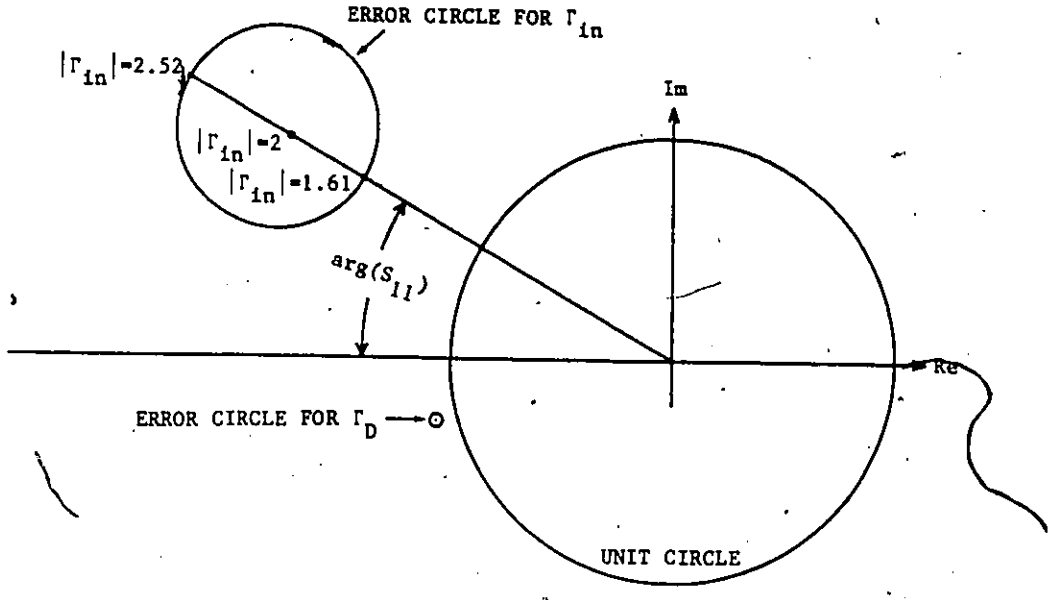

Fig. 3-3 The error circle for Γ_{in} when the error circle for Γ_D has a radius of 0.03.

The figure shows that the magnitude of Γ_{in} can lie anywhere between the extremes of $|\Gamma_{in}| = 2.52$ and $|\Gamma_{in}| = 1.61$ when Γ_D is allowed to move around its error circle of radius 0.03. Since $G = |\Gamma_{in}|^2$, the corresponding variation in gain is from G = 6.35 to G = 2.59.

Naturally, knowing that the predictability will improve as $|\Gamma_D|$ increases, the designer will want to obtain the largest possible $|\Gamma_D|$ from the diode. One way to do this, which is applicable to IMPATT diodes, is to use the largest safe bias current. Another way, which is applicable to all negative-

resistance devices, is to use the optimum transmission line impedance. It is shown in Appendix 1 that the largest $|\Gamma_D|$ will be measured when

$$Z_o = |Z_D| \tag{3-29}$$

where Z_o is the characteristic impedance of the transmission line, and Z_D is the diode impedance.

Since high-power amplifiers have low $|\Gamma_D|$, the design of high-power, high-gain amplifiers will require precise characterization of the diode for predictable results.

3-3 REFERENCES

[1] D.M.Kerns and R.W.Beatty, Basic Theory of Waveguide Junctions and Introductory Microwave Network Analysis. Oxford: Pergamon Press, 1967, pp. 46-48.

[2] S.J.Mason, "Feedback theory-further properties of signal flow graphs," Proc. IRE, vol. 44, no. 7, pp. 920-926, Jul. 1956.

4-1 SOME TRANSMISSION AMPLIFIER THEORY

Like the reflection amplifier, the transmission amplifier has a passband in which the gain is large and relatively constant. Unlike the reflection amplifier, the transmission amplifier is transmissive rather than reflective and reciprocal rather than nonreciprocal. Hence, this type of amplifier is essentially a filter with gain. The structure of any optimum filter that operates between identical impedances (or between identical waveguide cross sections) will be symmetrical about its center. Thus, the optimum single-diode transmission amplifier will have two symmetrically identical equalizers on each side of the diode as shown in Fig. 4-1a. (Here, optimum means the largest gain-bandwidth product is obtained from a given circuit complexity.)

Suppose a symmetrical single-diode transmission amplifier is driven at each port by signals that are equal in magnitude and phase. The circuit will then be structurally and electrically symmetrical and therefore indistinguishable from two identical and simultaneously operating reflection amplifiers. See Fig. 4-1b. This means that each equalizer can be designed as if it were meant for a reflection amplifier. In other words, the design of a transmission amplifier can be reduced to the design of a reflection amplifier. The apparent diode reflection coefficient for the reflection amplifiers can be derived from the actual diode S-paramaters as follows:

When the transmission amplifier is symmetrically driven, the incident and reflected waves on each side of the diode must satisfy eqs. (4-1). (See Fig. 4-1b.)

$$E_{1inc} = E_{2inc} \tag{4-1a}$$

$$E_{1ref} = E_{2ref} \tag{4-1b}$$

This means that the reflection coefficients seen looking toward

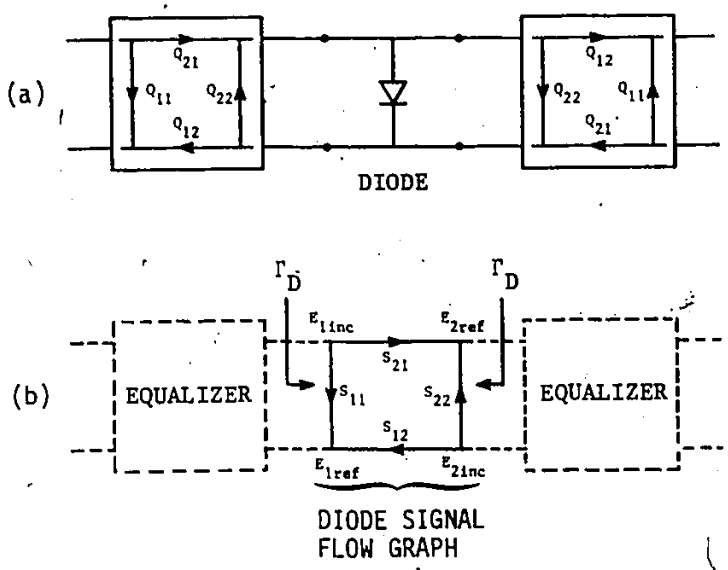

Fig. 4-1. (a)The symmetrical transmission amplifier. (b)The symmetrical transmission amplifier during simultaneous exitation. This amplifier behaves like two independent reflection amplifiers whose diode reflection coefficients are Γ_D.

the diode from either side are identical and equal to

$$\Gamma_D = E_{1ref}/E_{1inc} = E_{2ref}/E_{2inc} \tag{4-2}$$

Similarly, the reflection coefficients seen looking away from the diode are identical and equal to

$$E_{1inc}/E_{1ref} = E_{2inc}/E_{2ref} = 1/\Gamma_D \tag{4-3}$$

Applying eq. (3-18) to the diode gives

$$\Gamma_D = S_{11} + \frac{S_{21}S_{12}(1/\Gamma_D)}{1 - S_{22}(1/\Gamma_D)} \tag{4-4}$$

where S_{11}, S_{22}, S_{21}, and S_{12} are the diode S-parameters.

Because the diode is symmetrical and reciprocal

$$S_{11} = S_{22} \text{ and } S_{21} = S_{12} \tag{4-5}$$

The diode is shunt connected and electrically small. Thus the total voltage across the diode is just the sum of the incident and reflected waves or $1 + S_{11}$ (for unity incident voltage). Since the total voltage across the diode is also the value of the signal that is transmitted, one can immediately write

$$S_{21} = 1 + S_{11} \tag{4-6}$$

Substituting (4-5) and (4-6) into (4-4) gives

$$\Gamma_D^2 - 2S_{11}\Gamma_D - 1 - 2S_{11} = 0 \tag{4-7}$$

for which there are two solutions:

$$\Gamma_D = -1 \tag{4-8}$$

and

$$\Gamma_D = 2S_{11} + 1 \tag{4-9}$$

The first solution is a special case of the second solution ($S_{11} = -1$). The second solution gives the diode reflection coefficient to be used when designing a transmission amplifier by using methods appropriate for reflection amplifiers.

During simultaneous two way amplification, the diode must supply twice as much power as during one way amplification. (Equal input powers are assumed in both cases.) Since the diode is nonlinear, its parameters will be significantly different in

both cases. The optimum equalizers for simultaneous two-way transmission will not be same as those for one-way amplification. Therefore, equalizers designed by the method just described must use S_{11} as measured when the diode was adding the appropriate power for the application.

5-1 AN AMPLIFIER DESIGN EXAMPLE

The following example illustrates the design and behavior of the simple high-power reflection amplifier shown in Fig. 5-1. The

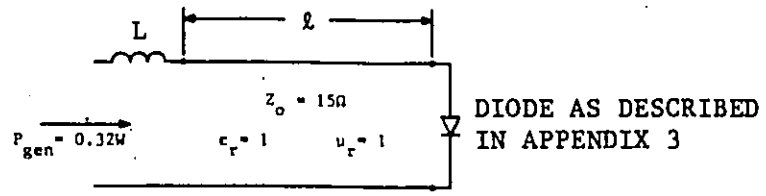

Fig. 5-1 A simple reflection amplifier design example. It is required to find the transmission line length ℓ and the inductance L so that there is a peak gain of 10 at 11 GHz.

diode is the ficticious X-band IMPATT diode described in Appendix 3. Its characteristic curves are repeated here in Fig. 5-2 for easy reference. It is required to obtain a peak gain of G = 10 at a frequency of f = 11 GHz when the input power is P_{gen} = 0.32 W.

The design of the equalizer rests on a knowledge of the power that the diode must add to the circuit to meet the specifications given above. From (3-5) this can be computed as

$$P_{add} = P_{gen}(G - 1) = 2.9 \text{ W} \tag{5-1}$$

Now that P_{add} is known, it is used to determine the incident power on the diode, P_{inc}, and the diode reflection coefficient, Γ_D. From (3-4) the incident power is

$$P_{inc} = P_{add}/(|\Gamma_D|^2 - 1) \tag{5-2}$$

Since P_{inc} and Γ_D are both unknown, a second relation involving them is required. It is represented by the characteristic curves for the diode. See Fig. 5-2. Usually

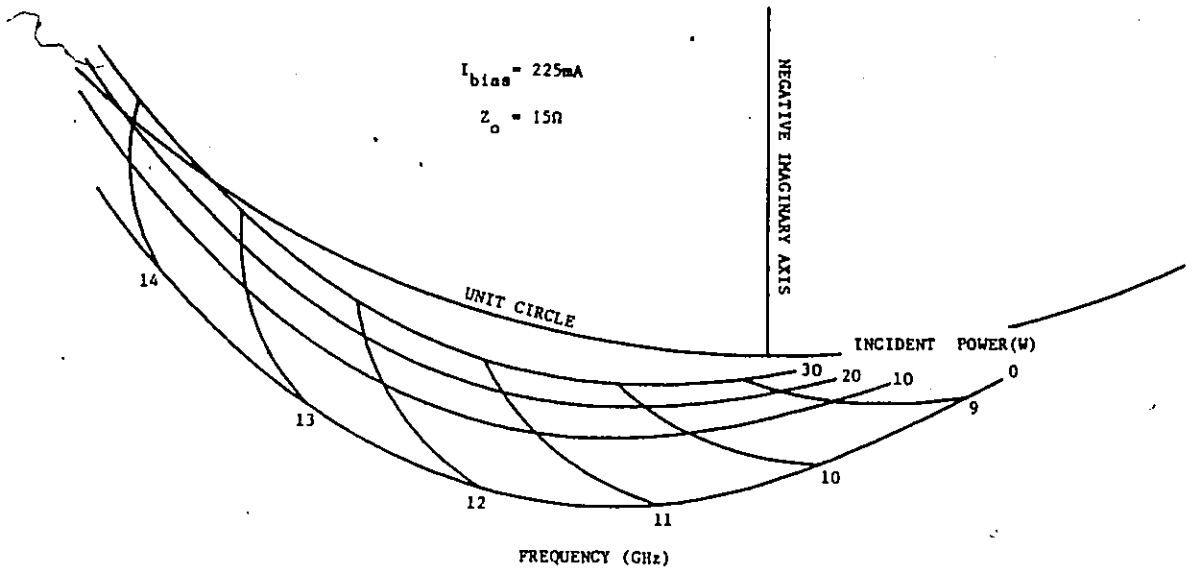

Fig. 5-2 Characteristic curves for the diode described in Appendix 3.

these curves are obtained by measurement, and then an explicit expression of the form

$$\Gamma_D = F(P_{inc}, f) \qquad (5\text{-}3)$$

is fitted to the results. For the purpose of this design example the function F is simulated by the Fortran program QWIKDIOD1 described in Appendix 3. This program returns Γ_D for a given P_{inc} and frequency f.

(5-2) and (5-3) can be solved for Γ_D by using the following recursion formula:

$$(P_{inc})_{n+1} = \frac{P_{add}}{|\, F[(P_{inc})_n, f]\,|^2 - 1}, \quad (P_{inc})_0 = 0 \qquad (5\text{-}4)$$

Γ_D is the value of F when the change in P_{inc} becomes negligible. For this example, Γ_D = -0.26 -j1.05 when P_{add}

= 2.9 W and f = 11 GHz.

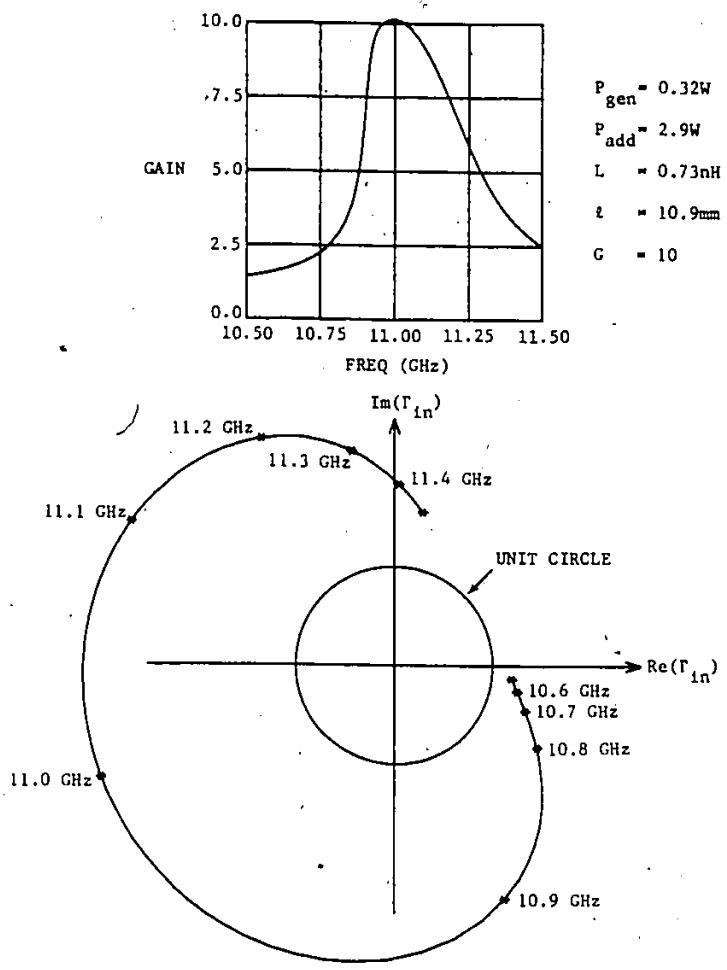

Fig. 5-3 Optimized gain and Γ_{in} functions for the example amplifier in Fig. 5-1.

Now that Γ_D is known, it can be used to determine S_{22} of

the equalizer. At frequencies near the center of the passband the phase of S_{22} can be found from (3-3a) and the magnitude of S_{22} can be found from (3-22).

Smith-chart techniques can be used to compute the size of the inductor that will present an equalizer reflection coefficient of S_{22} to the diode at 11 GHz. The results are

$$L = 0.7 \text{ nH} \tag{5-5}$$

and

$$\ell = 11 \text{ mm} \tag{5-6}$$

These are used as the starting point in an optimization routine to find the best fit to a flat gain of 10 between 10.9 GHz and 11.1 GHz. The optimized gain and Γ_{in} functions are plotted in Fig. 5-3. The optimum inductor size and position are also given.

5-2 THE INJECTION-LOCKED OSCILLATOR

The gain specification for this example was chosen so that the amplifier would behave as an injection-locked oscillator. The diode used in this example is somewhat more linear than a typical diode so a larger than typical gain was required to make the circuit oscillate when the input signal was removed.

As shown in Sec. 3-1, the condition for oscillation is that the loop gain in Fig. 3-1 is unity. This is written as

$$\Gamma_D S_{22} = 1 \tag{5-7a}$$

or, equivalently, as

$$S_{22} = 1/\Gamma_D \tag{5-7b}$$

Fig. 5-4 illustrates the behavior of an injection-locked oscillator by plotting the frequency dependence of both sides of (5-7b) in the complex plane.

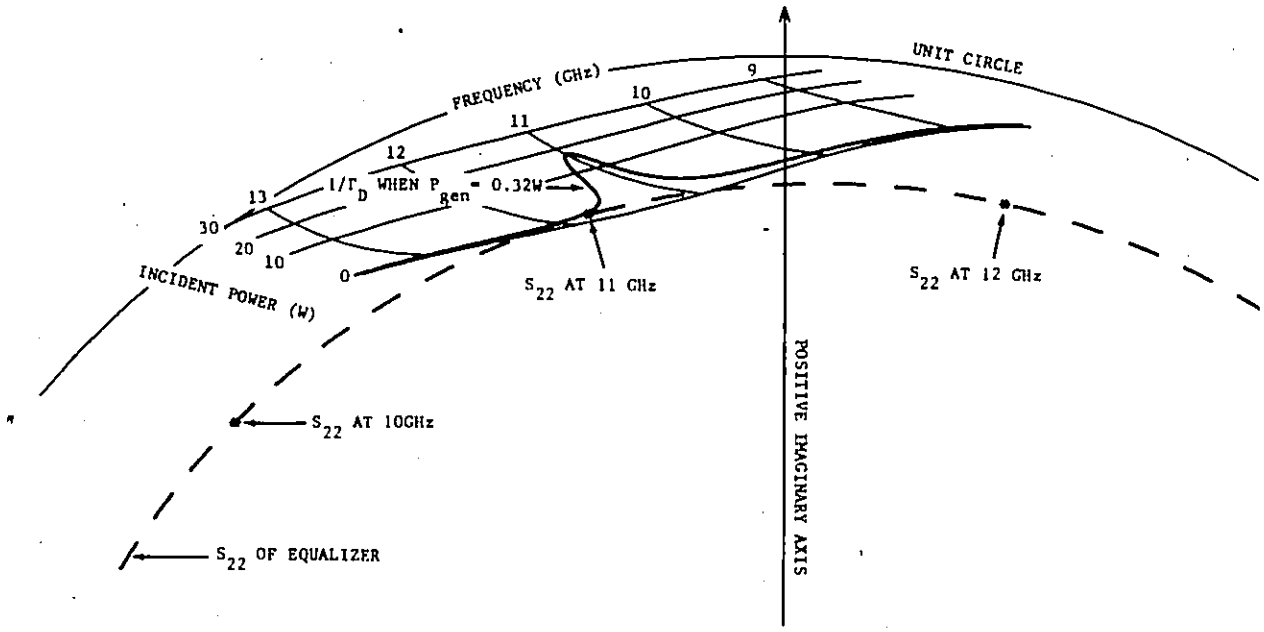

Fig. 5-4 The frequency dependent behavior of $1/\Gamma_D$ and S_{22} in the injection-locked oscillator/amplifier of Fig. 5-1.

Imagine that the circuit is amplifying according to the specifications given above. Also imagine that the frequency is being swept from below the passband to above the passband. S_{22} is seen to travel in a clockwise direction along the path indicated. Conversely, $1/\Gamma_D$ travels in a generally counterclockwise direction. Below the passband the path of $1/\Gamma_D$ approximates the characteristic curve for zero incident power. As the passband is traversed, the incident power seen by the diode increases and $1/\Gamma_D$ veers sharply away from the oncoming S_{22} (when P_{gen} = 0.32 W). At 11 GHz, S_{22} and $1/\Gamma_D$ have almost exactly the same phase, and the incident power is very near to maximum. Above the passband, the path of $1/\Gamma_D$ returns to the characteristic curve for zero incident

power.

This type of behavior can be seen in all reflection amplifiers, whether stable or injection locked.

That this amplifier <u>might</u> oscillate when there is no input signal is indicated by the presence of a portion of the path of S_{22} inside the region of operation of the diode. When there is no input signal, the path that would be followed by $1/\Gamma_D$ is the characteristic curve for $P_{inc} = 0$. That the amplifier <u>will</u> oscillate is indicated by the phase equality of S_{22} and $1/\Gamma_D$ when the frequency is ≈11.15 GHz. At this frequency, $|1/\Gamma_D| < |S_{22}|$. Therefore the total gain around the loop in Fig. 3-1 is real and greater than one. The loop signal, which is initially just a noise voltage, will increase continuously as it travels around the loop. At the same time P_{inc} will also increase since it is the power of the loop signal.

The incident power cannot increase forever. There must be some opposing mechanism that will eventually limit P_{inc} to some finite value. This mechanism reveals itself in the nonlinear behavior of the diode: Γ_D depends on P_{inc} in such a way that $1/|\Gamma_D|$ increases as P_{inc} increases. Thus, with each increase in P_{inc}, there is an opposing increase in $1/|\Gamma_D|$. This reduces the loop gain, causing P_{inc} to asymptotically approach a finite final value where the loop gain is one. At this value, eqs. (5-7) are satisfied and the circuit oscillates. From Fig. 5-4, the final value for P_{inc} in this example is about 1 W.

As long as there is no input signal, the circuit is a free-running oscillator. The output power of this oscillator is just the power added by the diode as calculated by (3-4).

$$P_{osc} = P_{add} = P_{inc} \left(|\Gamma_D|^2 - 1\right) \qquad (5\text{-}8)$$

To design a free-running oscillator, use the recursion formula (5-4) to find the Γ_D that occurs at the required power and frequency. Then, determine the necessary equalizer S_{22} from (5-7b). The rate at which S_{22} changes with frequency near the point $1/\Gamma_D$ determines the Q of the oscillator.

This amplifier design example was created to illustrate the behavior of a reflection amplifier operating under large signal conditions. The fin-line amplifier designed for this thesis was a small-signal amplifier because it was not possible to characterize the diode for large signal operation.

6-1 EQUALIZER DESIGN BY OPTIMIZATION

Today, computer assisted design (CAD) is widely used in microwave circuit design. An important part of CAD is computer optimization. This is the minimization of a function C that describes the closeness of fit of another function F to a desired function D. In the case of computer assisted equalizer design, D is the desired gain response of the amplifier and F is the calculated gain response for a particular set of variables. These variables can be lumped element values or the physical dimensions of a distributed element circuit.

There are many optimization routines in use today, each with its own unique set of advantages and disadvantages. Fortunately for the microwave circuit designer, the merits of each are relatively unimportant and any one routine will be adequate. One method of optimization proceeds by computing the gradient at some starting point and then following, more or less accurately, the path of steepest descent to the minimum. The Fortran code to implement this method for this thesis was adapted from the version of the Marquardt-Levenberg algorithm given in [1]. For a recent review of optimization techniques with a good list of references, refer to [2]

Obviously, it is desireable to select that starting point from which a steepest descent will lead to a global rather than a local minimum. It is the technique of selecting the starting point that distinguishes the various computer assisted equalizer design methods.

For example, those techniques [3], [4], [5] based on Carlin's resistance-excursion method [6] use a theorem from circuit theory to obtain the starting point for the optimization of lumped-element equalizers. (Carlin's method is also known as the real-frequency technique. An alternative description of the method can be found in [7].) The circuit can then be

transformed to an approximately equivalent distributed-element circuit appropriate for microwave frequencies.

Another technique, which is purely numerical, obtains a set of candidate starting points from a systematic search over a coarse n-dimensional grid defined by the n variables in F. Each of the candidates is then given to the optimization routine. The smallest of the minimums thus obtained is considered to be the global minimum. This approach is used in [8] and in this thesis. The listing of a Fortran subprogram for such a systematic search is given in [9].

This method's advantage is that it can give starting points directly in the form of microwave circuit dimensions; there is no need for an intermediate step involving lumped-element circuits and no need to learn techniques for transforming lumped circuits to distributed circuits.

For this thesis, the function to be minimized was defined as

$$C = \sum_{f=f_1}^{f_n} [F(f,d_1,d_2,\ldots,d_m) - D(f)]^2 \qquad (6\text{-}1)$$

where f_i, i = 1,n are frequencies equally spaced across the passband.

d_i, i = 1,m are the fin line circuit dimensions.

F is the computed gain function of the amplifier.

D is the desired flat gain function.

The gain and bandwidth of an amplifier cannot be selected independently of each other. That is, for any given passband

gain, G, the width of the passband cannot exceed a limit set by the diode reflection-coefficient function, $\Gamma_D(f)$, and the generator reflection-coefficient function, $\Gamma_G(f)$, [10], [11], [12]. For this reason the function D(f) must be chosen carefully so that the optimization routine is not asked to design an impossible equalizer. The feasibility of D(f) can be confirmed in advance by the techniques used in [10], [11], [12], [13], and [14], but the computations involved are intractable for all but the simplest Γ_D and Γ_G functions.

An alternative technique begins by optimizing an equalizer for a D(f) with a narrow and therefore feasible passband. The closeness of fit to D(f) will be better than required. The technique proceeds by repeating the optimization with progressively wider passbands until the closeness of fit is marginal. Typically three or four such iterations are all that are required. The bandwidth thus obtained is the largest realizable bandwidth for the chosen circuit complexity and type.

6-2 REFERENCES

[1] J.C.Nash, Compact Numerical Methods for Computers: linear algebra and function minimization. Bristol: Adam Hilger Ltd., 1979, pp. 175-177.

[2] U.L.Rohde, "CAD packages improve circuit optimization methods," Microwave Syst. News and Comm. Tech., vol. 15, No. 5, pp. 117-135, May 1985.

[3] H.J.Carlin and J.J.Komiak, "A new method of broad-band equalization applied to microwave amplifiers," IEEE Trans. Microwave Theory Tech., vol. MTT-27, pp. 93-99, Feb. 1979.

[4] H.J.Carlin and P.Amstutz, "On optimum broad-band matching," IEEE Trans. Circuits Syst., vol. CAS-28, pp. 401-405, May 1981.

[5] B.S.Yarman, "A simplified real frequency technique for broadband matching a complex generator to a complex load," RCA Review, vol. 43, pp. 529-540, Sep. 1982.

[6] H.J.Carlin, "A new approach to gain-bandwidth problems," IEEE Trans. Circuits Syst., vol. CAS-24, pp. 170-175, Apr. 1977.

[7] T.T.Ha, Solid-State Microwave Amplifier Design. New York: John Wiley & Sons, 1981, pp. 184-191.

[8] L.C.T.Liu and W.H.Ku, "Computer-aided synthesis of lumped lossy matching networks for monolithic microwave integrated circuits (MMIC's)," IEEE Trans. Microwave Theory Tech., vol. MTT-32, pp. 282-289, Mar. 1984.

[9] T.J.Aird and J.R.Rice, "Systematic search in high dimensional sets," SIAM J. Numerical Anal., vol.14, pp. 296-312, Apr. 1977.

[10] H.W.Bode, Network Analysis and Feedback Amplifier Design, New York: Van Nostrand, 1945, pp. 365-366, Sec. 16.3

[11] R.M.Fano, "Theoretical limitations on the broadband matching of arbitrary impedances," J. Franklin Inst., vol. 249, pp. 57-83, pp. 139-154; Jan. and Feb. 1950.

[12] D.C. Youla, "A new theory of broadband matching," IEEE Trans. Circuit Theory, pp. 30-50, Mar. 1964.

[13] D.C.Fielder, "Broad-band matching between load and source systems," IRE Trans. Circuit Theory, pp. 138-153, Jun. 1961.

[14] Ta-Mu Chien, "A theory of broadband matching of a frequency-dependent generator and load," J. Franklin Inst., vol. 208, pp. 181-221, Sept. 1974.

7-1 USING A NETWORK ANALYSER TO CHARACTERIZE STRUCTURES IN FIN LINE

Network analysers can directly measure the S-parameters of only those structures that are embedded in transmission media for which standard loads are available for calibration. Although there are no readily available standard loads for fin line, there is an indirect method that can be used to characterize fin-line structures.

The method begins by deducing the S-parameters of a transition to the transmission medium for which there are no standard loads. (In this thesis the transition was from rectangular waveguide to fin line.) Then, the structure to be characterized is placed between two such transitions, and the S-parameters of the combined circuit are measured. Finally, the S-parameters of the embedded structure are obtained by using deembedding formulas such as those given in Appendix 4.

For this thesis, the transition was characterized by a method similar to that described by Souza and Talboys [1] and by Gupta et al [2]. In their method, a set of 3 equations in S_{11}, S_{22}, and $S_{21}S_{12}$ are derived and then linearized by restricting the magnitude of S_{22} to nearly zero. (Although the solution of a linear set of equations is simple and straightforward, the restriction to $S_{22} \simeq 0$ can be avoided by solving the original nonlinear equations with an iterative technique.)

The method developed here obtains explicit (noniterative) expressions for S_{11}, S_{22}, and $S_{21}S_{12}$ without invoking the restriction $|S_{22}| \simeq 0$.

The derivation of this method begins by applying eq. (3-18) to the case of a 2-port terminated with a reflection coefficient of Γ_L. See Fig. 7-1. The result is

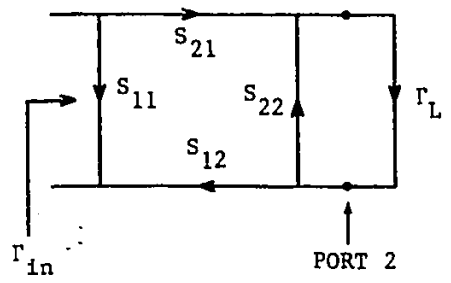

Fig. 7-1 The signal flow graph for a 2-port terminated with a reflection coefficient of Γ_L.

$$\Gamma_{in} = S_{11} + \frac{S_{21}S_{12}\Gamma_L}{1 - S_{22}\Gamma_L} \tag{7-1}$$

It is a simple although somewhat tedious task to obtain from (7-1) explicit formulas for S_{11}, S_{22}, and $S_{21}S_{12}$ in terms of 3 known pairs of reflection coefficients $(\Gamma_{inm}, \Gamma_{Lm})$, m = 1,3. These formulas are

$$S_{11} = \frac{FL - HJ}{HI - FK} \tag{7-2a}$$

$$S_{22} = -\frac{GI - EK}{HI - FK} \tag{7-2b}$$

$$S_{21}S_{12} = S_{11}S_{22} + \frac{EL - GJ}{HI - FK} \tag{7-2c}$$

where $E = \Gamma_{L2} - \Gamma_{L3}$

$F = \Gamma_{L1}(-E)$

$G = \Gamma_{L2} - \Gamma_{L1}$

$H = \Gamma_{L3}(-G)$

$I = \Gamma_{in2} - \Gamma_{in3}$

$J = \Gamma_{in1}(-I)$

$K = \Gamma_{in2} - \Gamma_{in1}$

$L = \Gamma_{in3}(-K)$

Eqs. (7-2) would appear to be inapplicable when the transmission medium at port 2 has no standard loads available for it. Fortunately, it is possible to induce known reflection coefficients without using a known physical termination:

A reflection coefficient of +1 appears at the axis of symmetry of a symmetrical 2-port when it is simultaneously driven at both ports by signals of equal magnitude and phase. A reflection coefficient of -1 appears when the driving signals are equal in magnitude but opposite in phase. Let each half of this 2-port be identical to the 2-port described in the previous paragraph so that ports 2 face each other. See Fig. 7-2a. There are now two pairs of (Γ_{in}, Γ_L) available for the characterization. They are obtained by measuring Γ_{in} during each type of exitation.

The third pair of (Γ_{in}, Γ_L) can be obtained after inserting a length of uniform transmission-line with the same cross-sectional geometry as that at port 2 of the original 2-port. See Fig. 7-2b. The resulting composite-2-port is still symmetrical, and reflection coefficients of +1 and -1 can be induced at the axis of symmetry as before. The reflection coefficient that terminates the original 2-port is just

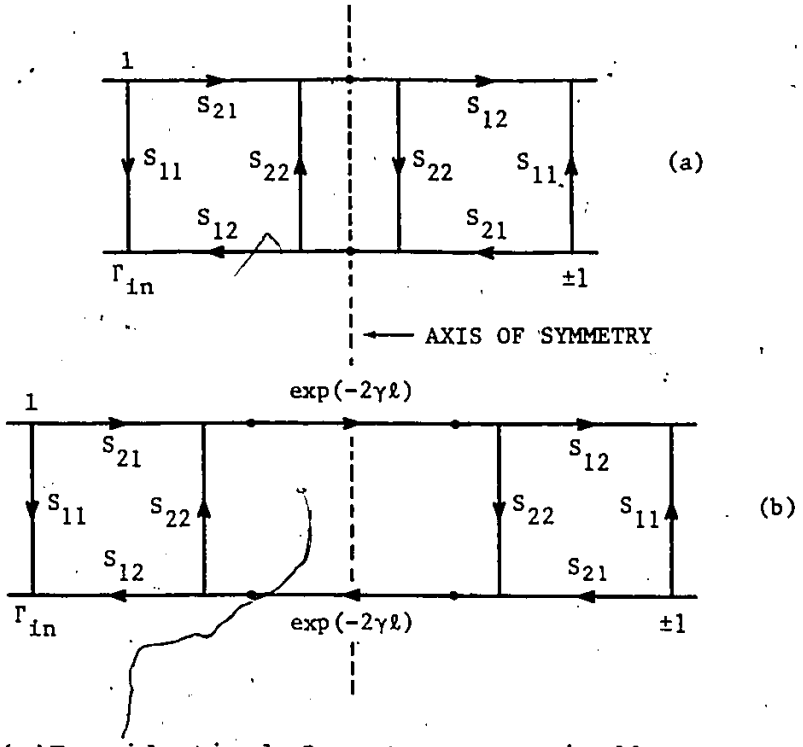

Fig. 7-2 (a)Two identical 2-ports symmetrically connected and driven so as to induce a reflection coefficient of ±1 at the axis of symmetry. (b)A uniform transmission-line is inserted at the axis of symmetry. The reflection coefficient at the axis of symmetry is still ±1 but the reflection coefficients at ports 2 have changed.

$$\Gamma_{L3} = \rho \exp(-2\gamma\ell) \qquad (7\text{-}3)$$

where

γ is the complex propagation constant of the transmission line.

ℓ is half the length of the transmission line.

ρ is the reflection coefficient induced at the axis of symmetry. The choice of $\rho = 1$ or $\rho = -1$ is arbitrary.

The pair (Γ_{in3}, Γ_{L3}) is obtained by measuring Γ_{in3} during either type of exitation. Eqs. (7-2) are then used to complete the characterization of the 2-port. Best experimental accuracy is obtained when 2ℓ is about one-quarter wavelength.

If the 2-port is known to be linear then the circuits of figure 2a,b need not be driven simultaneously. Instead, simultaneous exitation can be simulated by a computation based on the measured S-parameters of those circuits. The input reflection-coefficients that would have been measured during simultaneous in-phase and out-of-phase exitation are

$$\Gamma_{in} = R + T \qquad (7\text{-}4a)$$

and

$$\Gamma_{in} = R - T \qquad (7\text{-}4b)$$

respectively. R and T are the measured S_{11} and S_{21}, resp. of the symmetric circuit.

In this method, four measurements (two sets of R and T) are used to obtain the three parameters for the 2-port. This redundancy permits a reduction in experimental error. As shown in [3], each of the 2-port parameters can be determined as the average of four answers derived from the four possible combinations of the four pairs of (Γ_{in}, Γ_L) taken three at a time.

When an automatic network analyser is used, the extra measurement is obtained with no additional effort since this instrument normally gives its results in pairs of R and T.

Here is a summary of the procedure for characterizing a linear 2-port that has no standard loads available for one of its ports:

1.....Measure the S-parameters (R_a and T_a) of the circuit in Fig. 7-2a.

2.....Compute the first two pairs of (Γ_L, Γ_{in}) from

$$\Gamma_{in1} = R_a + T_a \,, \quad \Gamma_{L1} = +1 \tag{7-5a}$$

$$\Gamma_{in2} = R_a - T_a \,, \quad \Gamma_{L2} = -1 \tag{7-5b}$$

3.....Measure the S-parameters (R_b and T_b) of the circuit in Fig. 7-2b.

4.....Compute the third pair of (Γ_L, Γ_{in}) from

$$\Gamma_{in3} = R_b + T_b \,, \quad \Gamma_{L3} = \rho = 1 \exp(-2\gamma\ell) \tag{7-6a}$$

or from

$$\Gamma_{in3} = R_b - T_b \,, \quad \Gamma_{L3} = \rho = -1 \exp(-2\gamma\ell) \tag{7-6b}$$

5.....Use eqs. (7-2) to obtain S_{11}, S_{22}, and $S_{21}S_{12}$ with or without the averaging process described above.

7-2 CHARACTERIZING A WAVEGUIDE-TO-FIN-LINE TRANSITION

Fig. 7-3 contains diagrams of the two symmetrical circuits that were used to characterize the waveguide-to-fin-line transition. The inserted length of uniform fin-line was assumed to be lossless, hence γ in (7-3) became

$$\gamma = j(2\pi/\lambda_g) \tag{7-7}$$

λ_g, the guided wavelength in the uniform fin line, was computed from

$$\lambda_g/s = a_1 + a_2(s/\lambda) + a_3(s/\lambda)^2 + a_4(s/\lambda)^3 \tag{7-8}$$

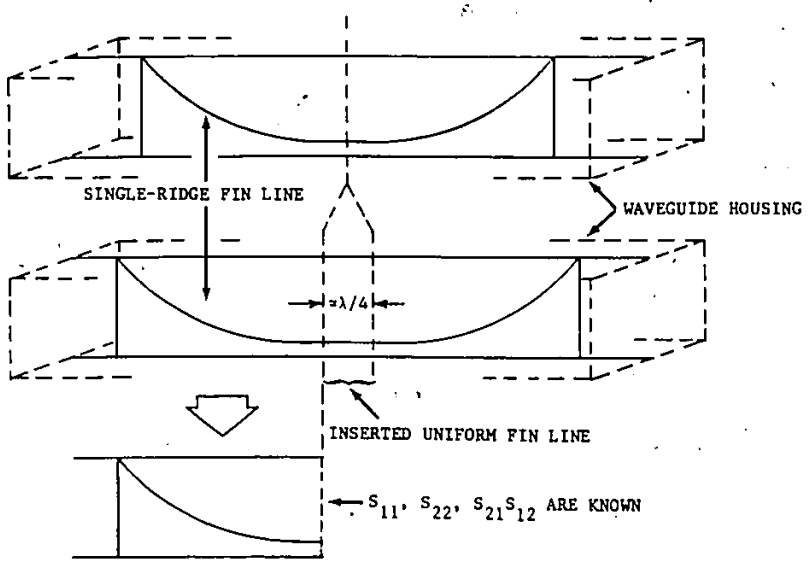

Fig. 7-3 The symmetrical circuits that were used to characterize the waveguide-to-fin-line transitions.

where $a_1 = 150.4 + 24.29\ (d/s)$ (7-9a)

$a_2 = -9092 - 2098\ (d/s)$ (7-9b)

$a_3 = 236500 + 64900\ (d/s)$ (7-9c)

$a_4 = -2269000 - 690800\ (d/s)$ (7-9d)

d is the gap width in the uniform fin line,

s is the fin line substrate thickness and

λ is the wavelength in free space.

This formula was obtained by fitting a polynomial to data obtained from a spectral domain program. The formula is within 1% of the data over the following ranges:

$s/a < 0.1$ (7-10a)

$0.6 < d/s < 2.7$ (7-10b)

$32 < \lambda/s < 49$ (7-10c)

where a is the broad dimension of the waveguide housing.

7-3 CHARACTERIZATION OF THE DIODE

Having found the characteristics of the waveguide-to-fin line transition, the diode S-parameters were obtained next by placing the diode between two such transitions. The S-parameters of the composite circuit were measured, and the diode S-parameters were deduced by using the deembedding formulas of Appendix 4.

S_{11} and S_{21} of the diode were used in (7-1) to obtain Γ_D, the reflection coefficient of the open-circuit terminated diode. The results are plotted in Fig. 7-4. The plot shows that the diode reflection coefficient lies very close to the unit circle. As was shown in Sec. 3-2, this is a very undesireable region for predictable amplifier design. This is a direct result of the large difference between the fin line impedance and the diode impedance. (Z_o of the fin line was about 100 ohms; the magnitude of the diode impedance was about 12 ohms.)

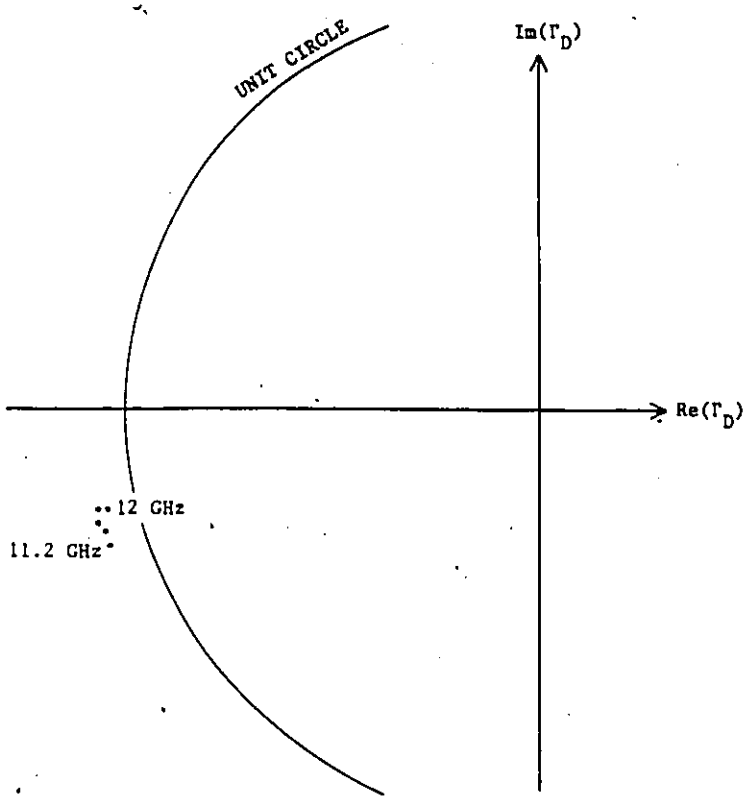

Fig. 7-4 Measured reflection coefficients of the open-circuit terminated diode in single-ridge unilateral fin line.

7-4 REFERENCES

[1] J.R.Souza and E.C.Talboys, "S-parameter characterization of coaxial to microstrip transition," IEE Proc., vol. 129, pt. H, no. 1, pp. 37-40, Feb. 1982.

[2] K.C.Gupta et al, Computer Aided Design of Microwave Circuits. Dedham: Artech House, 1981, pp. 319-321.

[3] R.F.Bauer and P.Penfield,Jr., "De-embedding and unterminating," IEEE Trans. Microwave Theory Tech., vol. MTT-22, pp. 282-288, Mar. 1974.

8-1 THE CHARACTERIZATION OF SERIES STUBS IN FIN LINE

The series stub has been a popular circuit element in the design of oscillators and narrow-band filters in fin line [1], [2]. However, until this thesis work, the available information did not have sufficient accuracy or flexibility for most other design problems. Before using the series stub in the fin line equalizer, it was necessary to obtain an improved description. Measurements were made at several frequencies on stubs of various lengths in unilateral fin lines with various gap widths to obtain a set of explicit expressions for stub S-parameters. The results represent a significant increase in the available design information for short- and open-circuited series stubs in fin line. (They have been published at the 1984 IEEE International Microwave Symposium [3].)

8-2 THE STUB MODEL

A fin line stub can be described either by its S-parameters or by an equivalent circuit with lumped elements. The latter has two advantages. First, it directly depicts the circuit behavior of the discontinuity. Second, it separately describes the various field disturbances at the branching points and at the far end of the stub.

These effects were incorporated into the equivalent transmission line circuits shown in Fig. 8-1. Then, measurements were made with an automatic network analyser to determine the dependence of the equivalent circuit parameters on frequency, stub length, and fin line gap width.

Like the diode, the series stubs were characterized by placing them between two waveguide-to-fin-line transitions as described earlier in Sec. 7-1. The transitions and stubs were etched on

0.76 mm thick RT/Duroid® (ε_r = 2.22) and mounted in WR-90 waveguide. See Fig. 8-2. All stubs had a width of 1 mm.

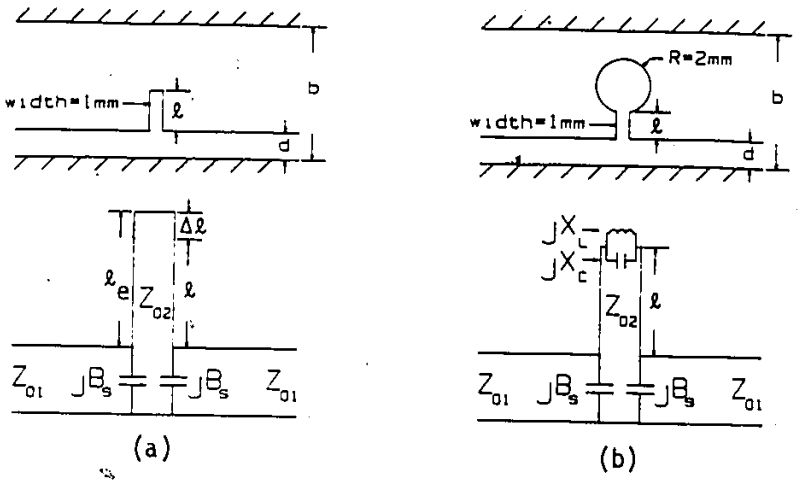

Fig. 8-1 Equivalent transmission line circuits for the short-(a) and open-(b) circuited series stubs in unilateral single-ridge fin line.

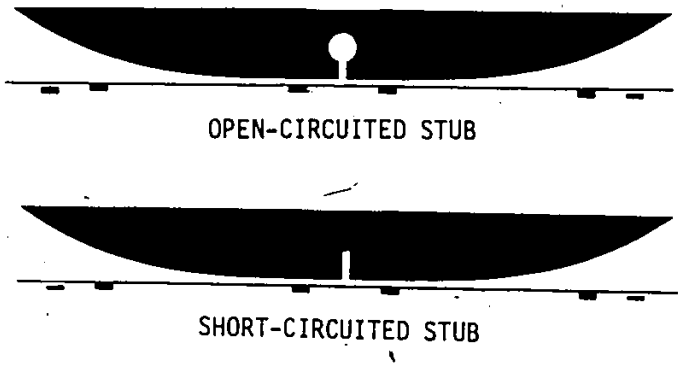

Fig. 8-2 Metalization patterns used to measure the scattering parameters of the stub discontinuities in unilateral fin line (WR-90, ε_r = 2.22, substrate thickness was s = 0.762 mm).

8-3 DERIVING THE EMPIRICAL EXPRESSIONS

The scattering parameters of an ideal series stub in a transmission line (that is, one with no losses and zero width and hence no branching points and end effects) are

$$S_{11s} = \frac{z_{in}}{2 + z_{in}} \tag{8-1}$$

$$S_{21s} = \frac{2}{2 + z_{in}} \tag{8-2}$$

where z_{in} is the impedance seen looking into the stub normalized to the characteristic impedance of the main transmission line. z_{in} can be computed from

$$z_{in} = z\,\frac{z_t + \tanh\gamma\ell_e}{1 + z_t\tanh\gamma\ell_e} \tag{8-3}$$

where z is the characteristic impedance of the stub divided by the characteristic impedance of the main transmission line, and
$\gamma = \alpha + j\beta$ is the propagation constant in the stub, and
ℓ_e is the length of the stub in the equivalent circuit, and
z_t is the terminating impedance of the stub divided by the characteristic impedance of the stub.

When a shunt admittance jB_s is added as shown in Fig. 8-1, the overall scattering parameters can be found from Mason's loop rule [4]. They are

$$S_{11} = S_{11b} + \frac{S_{21b}^2(S_{11s} - \Delta S_s S_{11b})}{1 - 2S_{11s}S_{11b} + \Delta S_s S_{11b}^2} \tag{8-4}$$

$$S_{21} = \frac{S_{21b}^2 S_{21s}}{1 - 2S_{11s}S_{11b} + \Delta S_s S_{11b}^2} \qquad (8\text{-}5)$$

where $S_{11b} = (-jb_s)/(2 + jb_s)$ is the reflection coefficient of a shunt admittance of $jb_s = jB_s Z_{01}$ (normalized to the characteristic admittance of the main transmission line, and

$S_{21b} = 1 + S_{11b}$ is the the transmission coefficient of the shunt admittance, and

$\Delta S_s = S_{11s}^2 - S_{21s}^2$

The following formulas were obtained by optimizing the fit of (8-4) and (8-5) to the experimental data for the series stubs. For convenience of scaling, all variables were normalized to the substrate thickness s.

$$b_s = 7.56(s/\lambda)\ \exp[-0.3117(d/s)] \qquad (8\text{-}6)$$

$$z = 2[1.524(d/s)]^{-0.594} \qquad (8\text{-}7)$$

$$\alpha = 0.08(s/\lambda)\ \text{nepers/mm} \qquad (8\text{-}8)$$

where λ is the free space wavelength.

The current flowing around the end of a short-circuited stub follows a path whose length is finite. This finite path length for the current gives the stub an inductive behavior which is modelled here by an excess length of line $\Delta\ell$ defined by

$$\Delta\ell/s = 0.1082(d/s)^2\ \{1 - \exp[-0.762(\ell/s)]\} \qquad (8\text{-}9)$$

Open-circuited stubs are terminated by a parallel combination of an inductive and capacitive reactance x_ℓ and x_c. See Fig. 8-1b. These reactances are normalized to the characteristic

impedance of the stub and are given by (8-10) and (8-11).

$$x_\ell = (s/\lambda)[84.12 - 2.474(\ell/s)] \qquad (8\text{-}10)$$

$$1/x_c = (s/\lambda)[30.93 - 7.422(\ell/s)][0.026 - 0.17(d/s)] \qquad (8\text{-}11)$$

(8-10) and (8-11) can be used to find the normalized terminating impedance

$$z_t = \frac{x_\ell x_a}{x_\ell + x_c} \qquad (8\text{-}12)$$

Expressions (8-6) to (8-11) are valid in the ranges given by (7-10) and in the range

$$1.6 < \ell/s < 5.3 \qquad (8\text{-}13)$$

When the error is computed as the magnitude of the difference between the fitted and measured scattering parameters, the standard deviation for the short-circuit fit is 0.03 and that for the open-circuit fit is 0.045. The reference planes of the scattering parameters are coincident with the stub edges.

The restriction to constant stub width allows simple expressions and should have little effect on the flexiblity of practical designs. Also, expressions (8-6) to (8-11) do not depend on the waveguide dimensions because small gap ratios ($d/b \ll 1$) and narrow substrates ($s/a \ll 1$) are assumed.

The expressions operate on normalized dimensions to allow convenient scaling to frequencies higher than X-band. Losses are expected to increase linearly with frequency as indicated by (8-8).

The wavelength in a stub can be computed from formula (7-8) for

the guided wavelength in a single ridge unilateral fin line on substrates with ε_r = 2.22. The wavelength is the same as that in single-ridge fin line when the fin-line gap is equal to half the stub width.

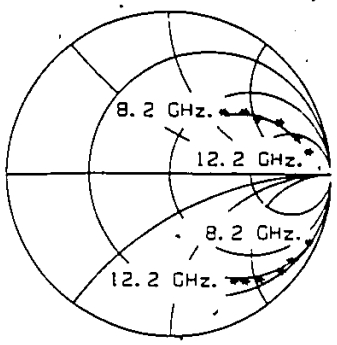

Fig. 8-3 Comparison of measured data to fitted curves for a short-circuited stub (inductive data) and an open-circuited stub (capacitive data). Each stub is 4 mm long and in a single-ridge unilateral fin line with fin line gap of 0.85 mm.

8-4 REFERENCES

[1] H.Hofmann, "MM-wave Gunn oscillator with disributed feedback fin-line circuit," Proc. 1980 MTT-S International Microwave Conference, pp. 59-61.

P.J.Meier, "Wideband subharmonically pumped W-band Mixer in single-ridge fin-line," 1982 IEEE MTT-S Digest, pp. 201-203.

[3] M.Burton and W.J.R.Hoefer, "An Improved Model for Short- and Open-Circuited Series Stubs in Fin Line," 1984 IEEE MTT-S Int'l Microwave Symp. Digest, pp. 330-332.

[4] S.J.Mason, "Feedback theory-further properties of signal flow graphs," Proc. IRE, vol. 44, no. 7, pp. 920-926, Jul. 1956.

9-1 A GENERAL DESCRIPTION OF THE FIN-LINE AMPLIFIER

The salient features of the fin-line amplifier that was designed for this thesis are shown in Fig. 9-1. Going from left to right there is a waveguide-to-fin-line transition, a fin line equalizer, the IMPATT diode, and a final series stub that presents an open circuit to the right side of the diode.

The waveguide-to-fin-line transition is not essential to the operation of the amplifier. Its purpose here is to permit characterization by a network analyser with waveguide test-ports. The fin line is single-ridged and unilateral with a teflon-fiberglass substrate (RT/Duroid®, $\varepsilon_r = 2.22$). There is a 1 mm. gap between the edge of the fin and the floor of the housing. Single-ridged fin line was used because it is the only type of fin line that allows one terminal of the diode to be mounted in the bulk metal of the housing for adequate heat sinking.

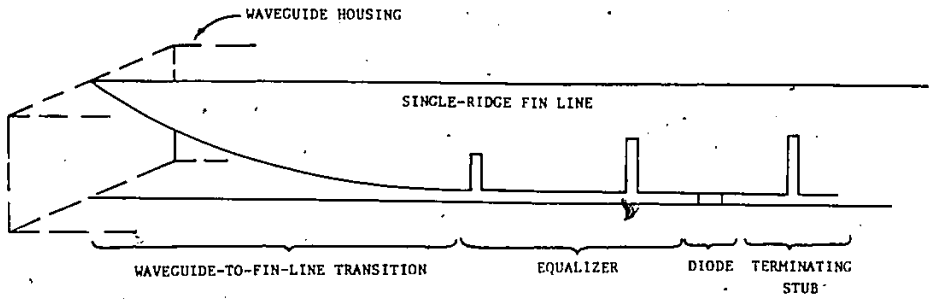

Fig. 9-1 The salient features of the fin-line amplifier.

The equalizer consists of two short-circuited stubs in series with the fin line. Their widths are 1 mm. Empirical results were used to characterize the stubs. Numerical results were used to characterize the lengths of uniform fin line that connect the stubs to each other and to the diode. Explicit formulas for the behavior of the stubs and of the uniform fin lines are presented

in Sec. 8-3 and Sec. 7-2, respectively.

The IMPATT diode is made by NEC (part no. ND8T11W-5H). This is a silicon diode capable of adding 3 W of power at 11 GHz. Its best dc-to-RF conversion efficiency is about 12%. Although the diode is capable of supplying high levels of RF power, the power levels prevailing in this amplifier were in the microwatt range. This is because both the amplifier and the diode were characterized with a network analyser whose test-port signal power was about 5μW. Such a small-signal amplifier is sufficient for the purpose of this thesis : to determine the feasibility of constructing an IMPATT amplifier in a fin line environment.

The series stub to the right of the diode serves to open-circuit terminate the right side of the diode. This method of termination allowed the local environment of the diode to be the same during the operation of the amplifier as during the characterization of the diode.

9-2 AMPLIFIER PERFORMANCE

The predicted and measured gain-curves for the amplifier are given in Fig. 9-2. There is agreement in the shape and location of the two curves, but there is a 3 dB difference in midband gain that needs to be explained. Since the measured and predicted passbands are in good agreement with respect to shape and location, it is unlikely that the gain error is due to phase errors in S_{22} or in Γ_D. (Refer to Sec 3-1 and the amplifier design example in Sec. 5-2.) Another possible explanation for the error in gain is that $|\Gamma_D|$ was smaller than the measured value. The sensitivity analysis of Sec. 3-2 shows that this explanation is likely given the uncertainty in Γ_D and the proximity of Γ_D to the unit circle:

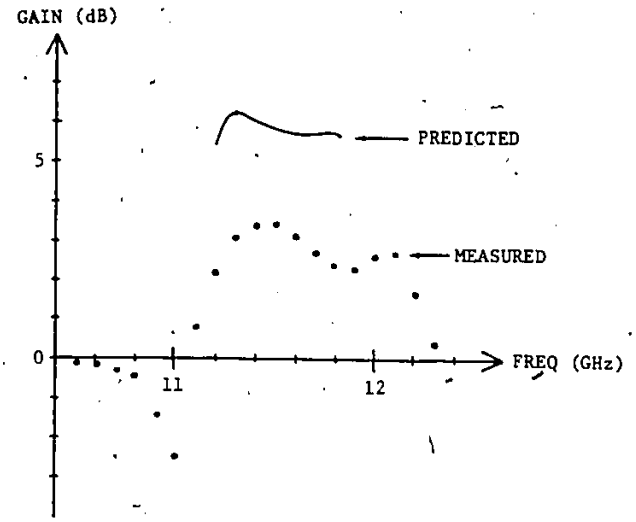

Fig. 9-2 Measured and predicted gain curves for the IMPATT amplifier in fin line.

A reasonable measure of the uncertainty in Γ_D comes from the results of the characterization of the fin-line stubs described in Chapt. 8. There, the magnitude of error between fitted and measured S-parameters for the shorted stubs had a standard deviation of 0.03. Since the same method and equipment were used to characterize the diode, the same standard deviation in magnitude of error can be assumed.

As shown in Fig. 7-4, the measured value for Γ_D is very close to the unit circle. This design used a midband value for Γ_D of -1.06 -j0.28.

Fig. 3-3 was created to illustrate the effects of exactly the conditions just described. It shows the circular path that Γ_{in} would follow as Γ_D is made to vary around its assumed value at a distance of 0.03. When $|\Gamma_D|$ is 0.03 less than its assumed value (arg[Γ_D] unchanged), the gain drops from 4 to 2.6. Thus, most of the error in gain can be

attributed to the small, but likely, magnitude error of 0.03 in $|\Gamma_D|$.

The poor predictability of this amplifier's performance is mostly due to the proximity of Γ_D to the unit circle. This in turn is due to the difference between the fin-line characteristic impedance and the magnitude of the diode impedance. (See Sec. 3-2.) The impedance of single-ridge fin line with a gap width of 1mm. is $Z_0 \simeq 100$ ohms. The magnitude of the diode impedance is $Z_D \simeq 15$ ohms. In theory, the fin-line impedance can be reduced to the optimum value of $Z_D = |Z_D|$. Γ_D would then be about four times further away from the unit circle (see Appendix 1), and the expected error in midband gain would be only 0.1 (assuming an experimental error of 0.03 in Γ_D). However, the appropriate fin-line gap is much too small for practical implementation even at such low frequencies as 11 GHz.

Another way to improve the predictability is to increase the accuracy of the diode characterization. Suppose the amplifier described here was allowed to have a 10% error in passband gain. That is, the gain is allowed to vary from as little as 3.6 to as much as 4.4. The corresponding variation in $|\Gamma_{in}|$ is from $\sqrt{3.6}=1.9$ to $\sqrt{4.4}=2.1$. Thus the error circle around Γ_{in} in Fig. 3-3 is allowed to have a radius of as much as 0.1. Theoretically an error circle of radius 0.1 around Γ_{in} would require an error-circle radius of only 0.007 around Γ_D. This requires a four-fold improvement in the accuracy of the characterization technique. Such accuracy would be very difficult to achieve at mm-wave frequencies. Also, such accuracy may become lost in the diode mounting uncertainties. The use of a low-impedance type of transmission line (such as microstrip) would allow $|\Gamma_D|$ to be maximized, and partially alleviates the need for excessive experimental accuracy.

The fin-line amplifier described here was a small-signal

amplifier; when the IMPATT amplifier is used in its normal function as a power amplifier the quantity $1 - |\Gamma_D|$ drops to about one-third of its small signal value. Hence, the requirement for precise characterization becomes difficult for microstrip and practically impossible for fin line.

For these reasons it can be concluded that the IMPATT diode and the fin line are an incompatible combination for negative resistance amplifiers.

10-1 CONCLUSIONS

In this thesis it was demonstrated that symmetrical single-diode transmission amplifiers can be designed by the same methods that are used to design reflection amplifiers.

An improved method is described for measuring the S-parameters of structures in transmission media such as fin line for which there are no standard loads.

Empirical expressions have been presented for the S-parameters of open- and short-circuited series stubs in single-ridge unilateral fin line. This is a significant contribution to the available design information for these structures because the effects of frequency, substrate thickness, fin line gap and stub length are incorporated.

The predictability of a negative-resistance amplifier improves as the required gain decreases and as the diode reflection coefficient moves away from the unit circle. This behavior is illustrated by the sensitivity curves in Fig. 3-2. The IMPATT diode and the fin line are not a suitable combination for negative-resistance amplification because the large fin-line impedance causes the diode reflection coefficient to reside very close to the unit circle. The maximum distance from Γ_D to the unit circle is obtained when the transmission-line impedance is equal to the magnitude of the diode impedance. It is not feasible to produce the small fin-line gap width required to match the impedance of the IMPATT diode.

APPENDIX 1

THE REFLECTION COEFFICIENT OF A DIODE AS A FUNCTION OF CHARACTERISTIC IMPEDANCE

The reflection coefficient of a diode at the end of a transmission line is

$$\Gamma_D = \frac{-Z_o + Z_D}{Z_o + Z_D} \qquad \text{(A1-1)}$$

where Z_o = transmission line characteristic impedance
Z_D = diode impedance

The purpose of this appendix is to show how Γ_D varies with Z_o for a given $Z_D = R_D + jX_D$. This can be done by computing the mapping of the real axis of the Z_o plane into the Γ_D plane.

Eq. (A1-1) is a mapping of the form

$$z = \frac{aw + b}{cw + d} \qquad \text{(A1-2)}$$

where $w = Z_o$
$a = -1$
$b = Z_D$
$c = 1$
$d = Z_D$

Finding the mapping of the real axis of the Z_o plane is equivalent to finding the locus of w in the z plane by varying $|w|$ and keeping arg[w] constant. It is shown in [1] that the locus is a circle with a radius of

$$R = \frac{|p|}{2|d/c| \sin(\arg[d] - \arg[c] - \arg[w])} \qquad \text{(A1-3)}$$

and center at

$$C = a/c + R \exp(j\{\arg[p] - \arg[w] + \pi/2\}) \qquad \text{(A1-4)}$$

where

$$p = (ad - bc)/c^2 \qquad \text{(A1-5)}$$

(Note : eq. 2.157 in [1] contains a miss printed sign.)

Using the equivalences given with (A1-2) gives

$$R = [1 + (R_D/X_D)^2]^{1/2} \qquad \text{(A1-6)}$$

and

$$C = -jR_D/X_D \qquad \text{(A1-7)}$$

Since the center of the circle in the Γ_D plane lies on the imaginary axis, the point where $|\Gamma_D|$ is largest must also lie on the imaginary axis. Thus, in (A1-1),

$$\arg[Z_D - Z_o] = \arg[Z_D + Z_o] \pm \pi/2 \qquad \text{(A1-8)}$$

when $|\Gamma_D|$ is largest. This means that the origin and the two points $Z_D - Z_o$ and $Z_D + Z_o$ form the vertices of a right triangle. (See Fig. A1-1.) The hypotenuse is the magnitude of the difference between these two vertices.

$$|(Z_D + Z_o) - (Z_D - Z_o)| = 2 Z_o \qquad \text{(A1-9)}$$

Application of the Pythagorean theorem to the triangle in Fig. A1-1 gives

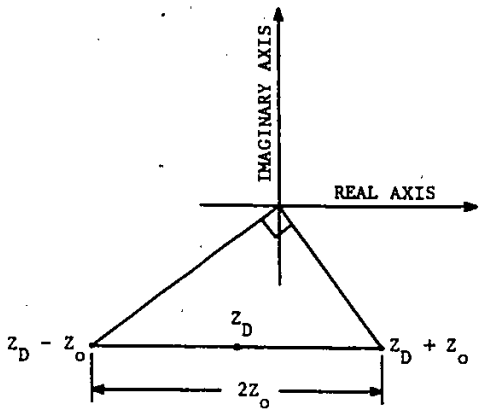

Fig. A1-1. The origin and the points $Z_D + Z_o$ and $Z_D - Z_o$ form a right triangle whose hypotenuse is $2Z_o$ in length.

$$|2Z_o|^2 = |Z_D + Z_o|^2 + |Z_D - Z_o|^2 \qquad \text{(A1-10)}$$

Inserting $Z_D = R_D + jX_D$ into (A1-10) and solving for Z_o gives

$$Z_o^2 = R_D^2 + X_D^2 \qquad \text{(A1-11)}$$

or

$$Z_o = |Z_D| \qquad \text{(A1-12)}$$

Thus for maximum $|\Gamma_D|$, Z_o must equal $|Z_D|$.

To illustrate the dependence of Γ_D on Z_o, the mapping in Fig. A1-2 was drawn. The diode impedance is the small signal impedance of the fictitious diode described in Appendix 3 (freq. = 11.6 GHz, I_{bias} = 225 mA). The quantity $1 - |\Gamma_D|$ diminishes by a factor of about four as Z_o goes from 15Ω to 100Ω.

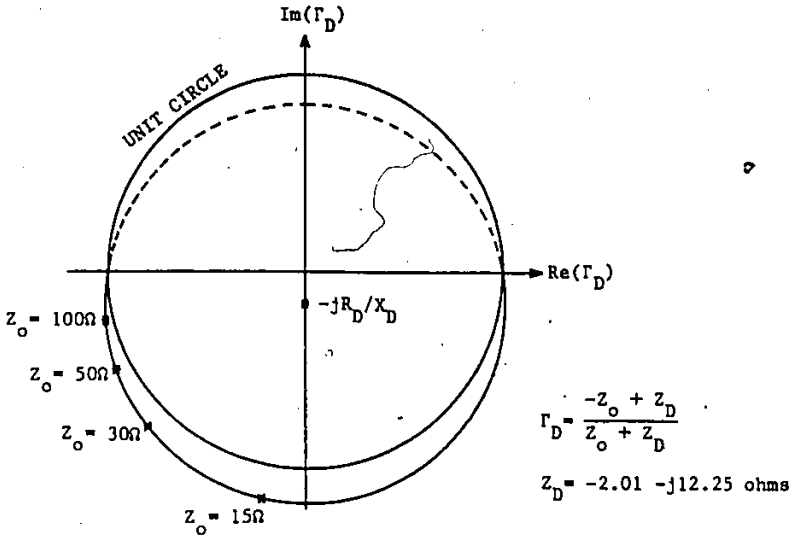

Fig. A1-2 A plot of Γ_D as function of Z_o. $|\Gamma_D|$ is largest when $Z_o = |Z_D|$.

REFERENCE

[1] D.M.Kerns and R.W.Beatty, Basic Theory of Waveguide Junctions and Introductory Microwave Network Analysis. Oxford: Pergamon Press, 1967, pp. 96-97.

APPENDIX 2

GENERAL FORMULAS FOR THE RADIUS AND CENTER OF A BILINEARLY TRANSFORMED CIRCLE

Eq. (A1-2) is known as the bilinear transformation. It has the property of mapping circles in the w-plane into circles in the z-plane. Whereas Appendix 1 gives the radius and center of the z-circle for the special case that the w-circle is a straight line through the origin (infinite radius and center at infinity), this appendix gives formulas for the radius and center in the general case.

The mapping (A1-2) is equivalent to

$$z = E + \frac{F}{w + G} \qquad \text{(A2-1)}$$

where $E = a/c$

$$F = \frac{bc - ad}{c^2}$$

$$G = d/c$$

Thus, to obtain the z-circle, the w-circle is first translated by G, then inverted, then stretched and rotated by F, and finally given another translation by E. Applying these operations to the w-circle with radius R_w and center at C_w leads to the following formulas for the radius R_z and the center C_z of the z-circle:

$$C_Z = E + F' \frac{H}{I} \qquad \text{(A2-2)}$$

$$R_Z = |F| \frac{|J|}{|I|} \qquad \text{(A2-3)}$$

where $H = K + L$

$$I = 2KL$$

$$J = K - L$$

$$K = M + \frac{R_w M}{|M|}$$

$$L = M - \frac{R_w M}{|M|}$$

$$M = C_w + G$$

APPENDIX 3

FORMULAS FOR THE IMPEDANCE OF A FICTITIOUS BUT TYPICAL IMPATT DIODE

The following two expressions describe the chip impedance of a typical silicon IMPATT DDR diode. They were created to aid the author's understanding of negative resistance amplifiers and oscillators. The expressions were derived by fitting to a variety of published experimental and theoretical curves for this type of diode. These expressions are believed to show the correct qualitative dependence on bias current, RF current, and frequency. Appropriate constants in the expressions were adjusted to give agreement with the manufacturer's data for the diode that was used in this thesis work (NEC ND8T11W-5H).

Chip reactance (ohms) :

$$X_D = -330/f \{ 1 - [1 - \exp(-I_{RF}/2.5)] [\exp((5-f)/4)] \} \qquad (A3\text{-}1)$$

Chip resistance (ohms) :

$$R_D = R_1 R_2 + 0.24\ I_{RF} \qquad (A3\text{-}2a)$$

where $$R_1 = 5 - \frac{9.4}{[1 + B^2]^{1/2}} \qquad (A3\text{-}2b)$$

$$R_2 = \frac{I_{BIAS}}{225} \left[1 - \frac{I_{RF}}{3.7}\right] \qquad (A3\text{-}2c)$$

$$B = \frac{A - 11}{3} \qquad (A3\text{-}2d)$$

$$A = f - 2\exp(6 - f) \qquad \text{(A3-2e)}$$

f = frequency in GHz.

I_{RF} = peak RF current through the chip in A.

I_{BIAS} = dc bias current through the chip in mA. The maximum safe bias current is 225 mA.

The maximum RF power available from this diode is 3.09 W at 11 GHz. This is also the maximum safe power for an IMPATT diode; driving a diode harder (increasing I_{RF}) actually reduces the power added and drastically increases the risk of failure. When (A3-2) is used in

$$\text{Power added} = -\tfrac{1}{2}(I_{RF})^2 R_D \quad , \; I_{BIAS} = 225 \; , \; f = 11 \qquad \text{(A3-3)}$$

the power added will increase with I_{RF} up to 3.09 W at I_{RF} = 2.05 A and then decrease beyond this point.

(A3-1) and (A3-2) can be computed by the Fortran subroutine Z_OF_IMPATT the listing for which appears at the end of this appendix.

The IMPATT diode chip is normally placed in a hermetically sealed package that adds additional parasitic reactances to form the total impedance of the packaged diode. The equivalent circuit for the packaged diode is shown in Fig. A3-1. The subroutine PACKAGED_DIODE computes the impedance of the packaged diode from the parasitics given in Fig. A3-1 and from the results of Z_OF_IMPATT. Also computed are the right and left side admittances and the diode reflection coefficient. These can be used to find the dependence of reflection coefficient on incident power. The listing for PACKAGED_DIODE appears at the end of this appendix.

At microwave frequencies, a useful method of characterizing

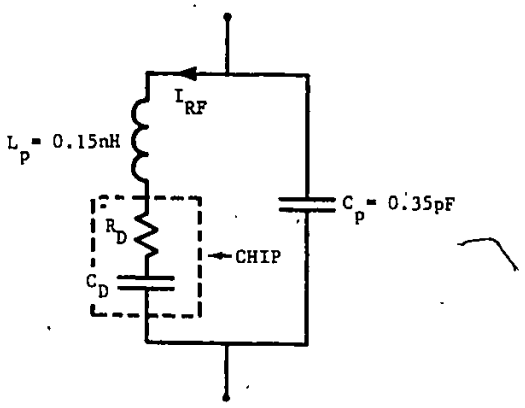

Fig. A3-1 The equivalent circuit for the fictitious diode. The package parasitics are the same as the published values for diode used in the fin line amplifier (NEC ND8T11W-5H).

nonlinear devices is to obtain their reflection coefficients for different incident power levels. To simulate this, a third program called QWIKDIOD1 was written to convert the impedance versus RF current description of the diode to a reflection coefficient versus incident power description. Because of the nonlinear interdependence of RF current, reflection coefficient and incident power, the reflection coefficient cannot be written as an explicit function of incident power. Instead, the program uses a method of successive approximations that becomes sufficiently accurate after less than six iterations. The results of this simulated characterization are presented in Fig. A3-2 as characteristic curves of Γ_D versus frequency for various incident power levels.

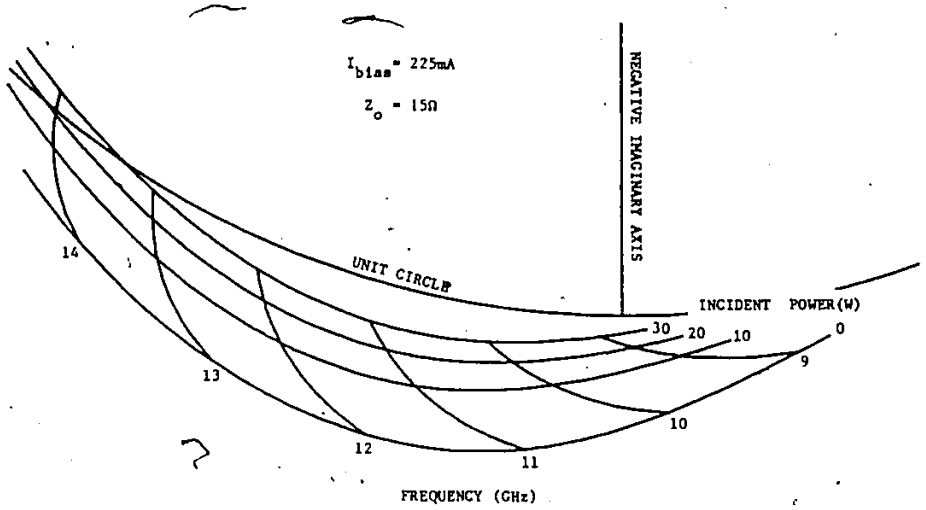

Fig. A3-2 Characteristic curves for the fictitious IMPATT diode.

The program listings for QWIKDIOD1, PACKAGED_DIODE, and Z_OF_IMPATT appear next:

```
0001    C               This program was written to convert the impedance versus
0002    C       RF current description of the diode to a reflection coefficient
0003    C       versus incident power description. It computes single values of peak rf
0004    C       current in the chip IRF and of power added by the diode PADDED when
0005    C       the diode is packaged and mounted at the end of a transmission line.
0006    C       The values of characteristic impedance Z0, bias current IBIAS,
0007    C       frequency FREQ, and incident power PINC are manually entered as the
0008    C       program runs. Diode refl. coeff. is also computed.
0009    C               The program is essentially a rapidly converging iteration
0010    C       that makes successively better approximations of the peak rf current
0011    C       in the chip after an initial guess of IRF = 0. Convergence to a
0012    C       tolerance TOLERANCE of .0001 in IRF typically occurs before the
0013    C       sixth iteration.
0014
0015
0016            REAL  LAST_IRF_CHIP, IRF_PKG, IRF_CHIP, IBIAS
0017            COMPLEX  REF_COEFF, Z_PKG, YLEFT, YRIGHT, Y_PKG
0018            INTEGER  COUNTER
0019
0020
0021    1       TYPE *
0022            TYPE 10
0023    10      FORMAT ('$ENTER Zo, Ibias, Freq , Pinc ,Tolerance !')
0024            ACCEPT *, ZO, IBIAS, FREQ, PINC, TOLERANCE
0025
0026            ROOT2 = SQRT(2.0)
0027            ROOTZO = SQRT(ZO)
0028
0029    C       Compute the magnitude of the incident voltage wave.
0030            A1 = SQRT( PINC )
0031
0032            LAST_IRF_CHIP = 0.0
0033            COUNTER = 0
0034            DELTA_IRF_CHIP = TOLERANCE + 1.0
0035
0036    C       Make successive approximations of the diode behavior until the
0037    C       change in peak rf current in the chip is less than TOLERANCE.
0038            DO WHILE (DELTA_IRF_CHIP .GT. TOLERANCE)
0039
0040    C       Use the last rf chip current to compute  a better approximation of
0041    C       the diode behavior.
0042            CALL PACKAGED_DIODE (ZO, FREQ, LAST_IRF_CHIP, IBIAS,
0043           1        REF_COEFF, YLEFT, YRIGHT, Y_PKG, Z_PKG)
0044
0045    C       Use the peak rf current at package terminals IRF_PKG to compute the
0046    C       the peak rf current through the chip IRF_CHIP.
0047            IRF_PKG = ROOT2 * A1/ROOTZO * CABS( 1.0 - REF_COEFF )
0048            IRF_CHIP = IRF_PKG * CABS( YLEFT/Y_PKG )
0049    C       Compute the difference between the chip current just computed and
0050    C       the chip current from the last iteration.
0051            DELTA_IRF_CHIP = ABS( LAST_IRF_CHIP - IRF_CHIP )
0052
0053            LAST_IRF_CHIP = IRF_CHIP
0054            COUNTER = COUNTER + 1
0055
0056            END DO
0057
```

```
0058     C       Compute the magnitude of the reflection coefficient.
0059             GAMMA = CABS( REF_COEFF )
0060
0061     C       Compute the power added by the diode.
0062             PADDED = PINC * (GAMMA*GAMMA - 1.0)
0063
0064     C       Print the results at the terminal.
0065             TYPE *
0066             TYPE *, 'Reflection coefficient =',REF_COEFF
0067             TYPE *, 'Padded = ',PADDED
0068             TYPE *, 'Irf = ',LAST_IRF_CHIP,'   Number of iterations is ',COUNTER
0069
0070
0071     C       Repeat for a new set of values for Z0, frequency, etc.
0072             GOTO 1
0073             END
```

PROGRAM SECTIONS

	Name	Bytes	Attributes
0	$CODE	451	PIC CON REL LCL SHR EXE RD NOWRT LONG
1	$PDATA	111	PIC CON REL LCL SHR NOEXE RD NOWRT LONG
2	$LOCAL	152	PIC CON REL LCL NOSHR NOEXE RD WRT QUAD
	Total Space Allocated	714	

ENTRY POINTS

Address	Type	Name
0-00000000		QWIKDIOD1$MAIN

VARIABLES

Address	Type	Name	Address	Type	Name
**	R*4	A1	**	I*4	COUNTER
**	R*4	DELTA_IRF_CHIP	2-00000034	R*4	FREQ
**	R*4	GAMMA	2-0000002C	R*4	IBIAS
**	R*4	IRF_CHIP	**	R*4	IRF_PKG
2-00000028	R*4	LAST_IRF_CHIP	**	R*4	PADDED
2-00000038	R*4	PINC	2-00000000	C*8	REF_COEFF
**	R*4	ROOT2	**	R*4	ROOTZ0
2-0000003C	R*4	TOLERANCE	2-00000010	C*8	YLEFT
2-00000018	C*8	YRIGHT	2-00000020	C*8	Y_PKG
2-00000030	R*4	Z0	2-00000008	C*8	Z_PKG

LABELS

Address	Label	Address	Label
0-00000018	1	1-00000042	10'

FUNCTIONS AND SUBROUTINES REFERENCED

Type	Name	Type	Name	Type	Name
R*4	MTH$CABS	R*4	MTH$SQRT		PACKAGED_DIODE

COMMAND QUALIFIERS

F/LIS QWIKDIOD1

/CHECK=(NOBOUNDS,OVERFLOW,NOUNDERFLOW)
/DEBUG=(NOSYMBOLS,TRACEBACK)
/STANDARD=(NOSYNTAX,NOSOURCE_FORM)
/SHOW=(NOPREPROCESSOR,NOINCLUDE,MAP,NODICTIONARY,SINGLE)
/WARNINGS=(GENERAL,NODECLARATIONS)
/CONTINUATIONS=19 /NOCROSS_REFERENCE /NOD_LINES /NOEXTEND_SOURCE /F77
/NOG_FLOATING /I4 /NOMACHINE_CODE /OPTIMIZE

COMPILATION STATISTICS

Run Time: 3.12 seconds
Elapsed Time: 9.57 seconds
Page Faults: 439
Dynamic Memory: 344 pages

```
0001            SUBROUTINE  PACKAGED_DIODE (Z0, F, IRF, IBIAS,
0002            1       REF_COEFF, YLEFT, YRIGHT, Y_PKG, Z_PKG)
0003
0004
0005    C       This subprogram computes the typical behavior of a packaged IMPATT
0006    C       diode designed for X-band. The diode is assumed to be mounted at
0007    C       the end of a transmission line of characteristic impedance Z0
0008    C       and the package capacitance CP incorporates the effect of the local
0009    C       geometry outside of the package. The package inductance LP is assumed
0010    C       to be unaffected by the external geometry.
0011    C               The behavior is given in terms of the reflection coefficient
0012    C       REF_COEFF, the left_hand (active) admittance YLEFT of the equivalent
0013    C       circuit, the right-hand admittance YRIGHT of the equivalent circuit,
0014    C       the total admittance at the package terminals Y_PKG, and the
0015    C       corresponding impedance at the package terminals Z_PKG.
0016    C               The behavior is a function of the characteristic impedance Z0,
0017    C       the frequency F, the peak rf current in the chip IRF, and the bias
0018    C       current IBIAS. Although the peak rf current in the chip is assumed
0019    C       to be already known , it is actually a function of the characteristic
0020    C       impedance and the incident power. Thus, to compute the diode behavior
0021    C       as a function of incident power this subprogram can be used in an
0022    C       iteration that makes successively better approximations of the diode
0023    C       behavior by repeatedly revising the RF chip current from an initial
0024    C       guess of IRF = 0.
0025    C               F is in GHz., IRF is in A., and IBIAS is in mA.
0026
0027            COMPLEX  REF_COEFF, ZLEFT, YLEFT, YRIGHT, Y_PKG, Z_PKG
0028            COMPLEX  Z_OF_IMPATT
0029            REAL  LP, IRF, IBIAS
0030
0031            PARAMETER (TWO_PI=6.2832, PI=3.1416, CP=0.35E-3, LP=0.15)
0032
0033    C       Compute the characteristic admittance Y0.
0034            Y0 = 1.0 / Z0
0035
0036    C       Compute the left_hand admittance from the left_hand impedance ZLEFT.
0037    C       ZLEFT is the sum of the chip impedance and the parasitic inductive
0038    C       reactance of the package.
0039            ZLEFT = Z_OF_IMPATT (F, IRF, IBIAS) + CMPLX (0.0, TWO_PI*F*LP)
0040            YLEFT = 1.0 / ZLEFT
0041
0042    C       Compute the right hand admittance.
0043            YRIGHT = CMPLX( 0.0, TWO_PI*F*CP )
0044
0045    C       Compute the total admittance and the corresponding impedance.
0046            Y_PKG = YRIGHT + YLEFT
0047            Z_PKG = 1.0 / Y_PKG
0048
0049    C       Compute the reflection coefficient.
0050            REF_COEFF = (Y0 - Y_PKG) / (Y0 + Y_PKG)
0051
0052            END
```

PROGRAM SECTIONS

	Name	Bytes	Attributes
0	$CODE	213	PIC CON REL LCL SHR EXE RD NOWRT LONG
2	$LOCAL	28	PIC CON REL LCL NOSHR NOEXE RD WRT QUAD
	Total Space Allocated	241	

ENTRY POINTS

Address	Type	Name
0-00000000		PACKAGED_DIODE

VARIABLES

Address	Type	Name	Address	Type	Name	Address	Type	Name	Address	Type	Name
AP-000000088	R*4	F	AP-000000108	R*4	IBIAS	AP-0000000C8	R*4	IRF	AP-000000148	C*8	REF_COEFF
2-00000008	R*4	Y0	AP-000000188	C*8	YLEFT	AP-0000001C8	C*8	YRIGHT	AP-000000208	C*8	Y_PKG
AP-000000048	R*4	Z0	2-00000000	C*8	ZLEFT	AP-000000248	C*8	Z_PKG			

FUNCTIONS AND SUBROUTINES REFERENCED

Type	Name
C*8	Z_OF_IMPATT

COMMAND QUALIFIERS

```
F/LIS/NOOP PKGDIODE

/CHECK=(NOBOUNDS,OVERFLOW,NOUNDERFLOW)
/DEBUG=(NOSYMBOLS,TRACEBACK)
/STANDARD=(NOSYNTAX,NOSOURCE_FORM)
/SHOW=(NOPREPROCESSOR,NOINCLUDE,MAP,NODICTIONARY,SINGLE)
/WARNINGS=(GENERAL,NODECLARATIONS)
/CONTINUATIONS=19  /NOCROSS_REFERENCE  /NOD_LINES  /NOEXTEND_SOURCE  /F77
/NOG_FLOATING  /I4  /NOMACHINE_CODE  /NOOPTIMIZE
```

COMPILATION STATISTICS

```
Run Time:          1.81 seconds
Elapsed Time:      4.04 seconds
Page Faults:       274
Dynamic Memory:    328 pages
```

```
0001            COMPLEX FUNCTION  Z_OF_IMPATT (FREQ, IRF, IBIAS)
0002            
0003    C               This subprogram computes the impedance of an IMPATT diode chip
0004    C       designed for operation at X-band. The formulas for chip resistance RD
0005    C       and chip reactance XD show a dependence on frequency FREQ , bias
0006    C       current IBIAS, and peak rf current IRF that is typical of a silicon
0007    C       DDR diode. The maximum power generated by the diode is 3.09 W. at
0008    C       11 GHz. with peak rf current of 2.051 A. The corresponding chip
0009    C       resistance is -1.47 ohms.
0010    C               This subroutine is called by subprogram PACKAGED_DIODE to
0011    C       compute the behavior the packaged chip when it is mounted at the end of
0012    C       a transmission line.
0013    C               Frequency is in GHz., bias current is in mA., and the peak
0014    C       rf current is in A.
0015            
0016            REAL IBIAS, IBIAS_OP, IRF
0017            
0018            PARAMETER  (IBIAS_OP = 225.0)
0019            
0020            
0021            XD = -330.0 / FREQ * (1.0 - (1.0 - EXP( -IRF/2.5 )) *
0022           1       EXP((5.0 - FREQ) / 4.0))
0023            
0024            FF = FREQ - 2.0 * EXP(6.0 - FREQ)
0025            PP = (FF - 11.0) / 3.0
0026            R1 = -9.4 / SQRT( 1.0 + PP*PP ) + 5.0
0027            
0028            R2 = IBIAS/IBIAS_OP * ( 1.0 - IRF/3.7 )
0029            
0030            RD = R1*R2 + 0.24*IRF
0031            
0032            Z_OF_IMPATT = CMPLX( RD, XD )
0033            
0034            END
```

PROGRAM SECTIONS

	Name	Bytes	Attributes
0	$CODE	180	PIC CON REL LCL SHR EXE RD NOWRT LONG
2	$LOCAL	32	PIC CON REL LCL NOSHR NOEXE RD WRT QUAD
	Total Space Allocated	212	

ENTRY POINTS

Address	Type	Name
0-00000000	C*8	Z_OF_IMPATT

VARIABLES

Address	Type	Name	Address	Type	Name	Address	Type	Name	Address	Type	Name
2-0000000C	R*4	FF	AP-00000040	R*4	FREQ	AP-0000000C	R*4	IRIAS	AP-00000008	R*4	IRF
2-00000010	R*4	PP	2-00000014	R*4	R1	2-00000018	R*4	R2	2-0000001C	R*4	RD
2-00000008	R*4	XD									

FUNCTIONS AND SUBROUTINES REFERENCED

Type	Name	Type	Name
R*4	MTH$EXP	R*4	MTH$SORT

COMMAND QUALIFIERS

```
F/LIS/NOOP ZIMPATT

/CHECK=(NOBOUNDS,OVERFLOW,NOUNDERFLOW)
/DEBUG=(NOSYMBOLS,TRACEBACK)
/STANDARD=(NOSYNTAX,NOSOURCE_FORM)
/SHOW=(NOPREPROCESSOR,NOINCLUDE,MAP,NODICTIONARY,SINGLE)
/WARNINGS=(GENERAL,NODECLARATIONS)
/CONTINUATIONS=19  /NOCROSS_REFERENCE  /NOD_LINES  /NOEXTEND_SOURCE  /F77
/NOG_FLOATING  /I4  /NOMACHINE_CODE  /NOOPTIMIZE
```

COMPILATION STATISTICS

Run Time:	1.73 seconds
Elapsed Time:	4.11 seconds
Page Faults:	188
Dynamic Memory:	320 pages

APPENDIX 4

THE DE-EMBEDDING FORMULAS OF KRUPPA AND SODOMSKY

The S-parameters of the unknown 2-port in Fig. A4-1 can be determined from the S-parameters of the embedding 2-ports and from the measured S-parameters of the cascade of 2-ports. Explicit formulas for the S-parameters of the embedded 2-port are [1]

$$S_{11} = \frac{(R_F - S_{11}^{(1)})[S_{22}^{(2)}(R_R - S_{11}^{(2)}) + S_{21}^{(2)}S_{12}^{(2)}] - S_{22}^{(2)}T_R T_F}{D} \qquad \text{(A4-1)}$$

$$S_{12} = \frac{T_R S_{21}^{(1)} S_{12}^{(2)}}{D} \qquad \text{(A4-2)}$$

$$S_{21} = \frac{T_F S_{21}^{(2)} S_{12}^{(1)}}{D} \qquad \text{(A4-3)}$$

$$S_{22} = \frac{(R_R - S_{11}^{(2)})[S_{22}^{(1)}(R_F - S_{11}^{(1)}) + S_{21}^{(1)}S_{12}^{(1)}] - S_{22}^{(1)}T_R T_F}{D} \qquad \text{(A4-4)}$$

where $D = UV - W$

$$U = S_{12}^{(1)}S_{21}^{(1)} + S_{22}^{(1)}(R_F - S_{11}^{(1)})$$

$$V = S_{21}^{(2)}S_{12}^{(2)} + S_{22}^{(2)}(R_R - S_{11}^{(2)})$$

$$W = S_{22}^{(2)}S_{22}^{(1)}T_R T_F$$

R_F, T_F, R_R, and T_R are the measured S-parameters of the composite circuit in Fig. A4-1. R_F and T_F are the reflection

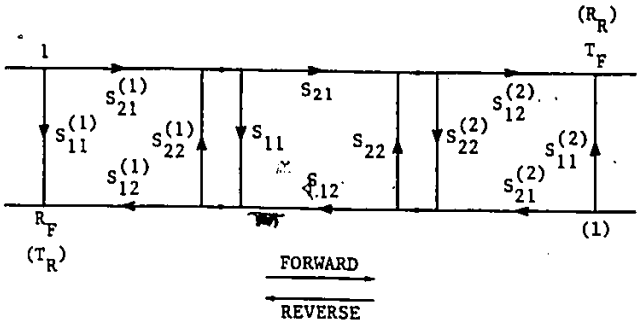

Fig. A4-1 An unknown 2-port embedded between two known 2-ports. The forward S-parameters of the entire cascade are R_F and T_F. The reverse S-paramters are R_R and T_R.

and transmission S-parameters, resp. measured in the forward direction (left to right in the figure). R_R and T_R are the reflection and transmission S-parameters, resp. measured in the reverse direction (right to left in the figure).

REFERENCE

[1] W.Kruppa and K.F.Sodomsky, "An explicit solution for the scattering parameters of a linear two-port measured with an imperfect test set," IEEE Trans. Microwave Theory Tech., vol. MTT-19, pp. 122-123, Jan. 1971.

APPENDIX 5

A DETERMINATION OF THE RANGE OF S_{22} FOR A LOSSLESS EQUALIZER THAT WILL OBTAIN THE REQUIRED GAIN FROM A NEGATIVE-RESISTANCE DEVICE

In Sec. 3-1 it is shown that, when a lossless equalizer is connected to a negative-resistance device (N.R.D.), the circuit must satisfy the the following restriction:

$$|1 - \Gamma_D S_{22}|^2 = K(1 - |S_{22}|^2) \qquad \text{(A5-1)}$$

where $K = \dfrac{|\Gamma_D|^2 - 1}{G - 1}$

G = amplifier gain

Γ_D = reflection coefficient of the N.R.D.

S_{22} = match terminated reflection coefficient of the lossless equalizer as seen by the N.R.D.

The squared magnitude of $1 - \Gamma_D S_{22}$ can be obtained by a direct application of the cosine law. The result is

$$1 + |\Gamma_D S_{22}|^2 - 2|\Gamma_D S_{22}|\cos(\alpha) = K(1 - |S_{22}|^2) \qquad \text{(A5-2)}$$

where $\alpha = \arg[\Gamma_D] + \arg[S_{22}]$

Isolating $\cos(\alpha)$ and simplifying gives

$$\cos(\alpha) = \frac{1 - K}{2|\Gamma_D||S_{22}|} + \frac{(|\Gamma_D|^2 + K)|S_{22}|}{2|\Gamma_D|} \qquad \text{(A5-3)}$$

Since $\cos(\alpha)$ must be less than or equal to one, the limits for $|S_{22}|$ can be found by solving

$$1 = \frac{1 - K}{2|\Gamma_D||S_{22}|} + \frac{(|\Gamma_D|^2 + K)|S_{22}|}{2|\Gamma_D|} \qquad \text{(A5-4)}$$

for $|S_{22}|$. The two solutions are

$$|S_{22}| = \frac{|\Gamma_D| \pm (K^2 + |\Gamma_D|^2 K - K)^{1/2}}{|\Gamma_D|^2 + K} \qquad \text{(A5-5)}$$

When S_{22} is within these limits, its argument can be found from

$$\arg[S_{22}] = \alpha - \arg[\Gamma_D] \qquad \text{(A5-6)}$$